THE JOURNAL OF ACOUSTICAL SOCIETY OF INDIA

Volume 45   **Number 1**   **January 2018**

A Quarterly Publication of the ASI
http://www.acousticsindia.org

The Journal of Acoustical Society of India

The Refereed Journal of the Acoustical Society of India (JASI)

The Journal of Acoustical Society of India is a refereed journal of the Acoustical Society of India **(ASI)**. The **ASI** is a non-profit national society founded in 31st July, 1971. The primary objective of the society is to advance the science of acoustics by creating an organization that is responsive to the needs of scientists and engineers concerned with acoustics problems all around the world.

Manuscripts of articles, technical notes and letter to the editor should be submitted to the Chief Editor. Copies of articles on specific topics listed above should also be submitted to the respective Associate Scientific Editor. Manuscripts are refereed by at least two referees and are reviewed by Publication Committee (all editors) before acceptance. On acceptance, revised articles with the text and figures scanned as separate files on a diskette should be submitted to the Editor by express mail. Manuscripts of articles must be prepared in strict accordance with the author instructions.

All information concerning subscription, new books, journals, conferences, etc. should be submitted to Chief Editor:

B. Chakraborty, CSIR - National Institute of Oceanography, Dona Paula, Goa-403 004,
Tel: +91.832.2450.318, Fax: +91.832.2450.602, e-mail: bishwajit@nio.org

Annual subscription price including mail postage is Rs. 2500/= for institutions, companies and libraries and Rs. 2500/= for individuals who are not **ASI** members. The Journal of Acoustical Society of India will be sent to **ASI** members free of any extra charge. Requests for specimen copies and claims for missing issues as well as address changes should be sent to the Editorial Office:

ASI Secretariat, C/o Acoustics, Ultrasonics & Vibration Section, CSIR-National Physical Laboratory, Dr. KS Krishnan Road,
New Delhi 110 012, Tel: +91.11.4560.8317, Fax: +91.11.4560.9310, e-mail: asisecretariat.india@gmail.com

The Journal of Acoustical Society of India

A quarterly publication of the Acoustical Society of India

Volume 45, Number 1, January 2018

ARTICLES

INFORMATION

Acoustic source localization accuracy using network of sonobuoys of omni-directional hydrophones and acoustic vector sensors

Bipin Kumar, Arun Kumar and Rajendar Bahl
Centre for Applied Research in Electronics
Indian Institute of Technology, Delhi-110016, India
crz148292@iitd.ac.in

ABSTRACT

We have done simulation studies to compare the localization accuracy of an underwater radiating acoustic source using omni-directional hydrophone based sonobuoys and acoustic vector sensor(AVS) based sonobuoys, without and with an interference source for the same number of sonobuoys of either type. We use Time Difference of Arrival (TDOA) method for hydrophone sonobuoys and Direction of Arrival (DOA) based method for AVS sonobuoys to localize the target. The analysis is shown for isotropic colored Gaussian noise for sea-state3. The performance has been evaluated in terms of Root Mean Square Error. We have done the simulation study for sonobuoy placement in circular and L-shape geometries, by varying the inter-element spacing and SNR of the target. Also, the effects of placing the sonobuoys close or far apart and influence of interference sources on localization accuracy are studied and inferences are drawn. It is shown that the AVS based sonobuoys offer advantages in terms of improved localization accuracy compared to omni-directional hydrophone based sonobuoys.

1. INTRODUCTION

An Acoustic Vector Sensor (AVS) is a sensor that measures acoustic pressure as well as the components of acoustic particle velocity at a collocated point. An AVS, in most general form, comprises of three orthogonally oriented particle velocity sensors and an optional hydrophone, all spatially collocated in a point like geometry. Each velocity sensor has an intrinsic directional response to the incident sound field. A single point measurement using a conventional hydrophone yields only the scalar information on the sound field, viz. the pressure amplitude. On the other hand, the particle velocity measurements in an AVS provide additional information about the acoustic field, which is not available in the case of a single hydrophone. This gives the AVS many advantages over hydrophones such as compactness, better and unambiguous localization for underwater acoustic sensing applications and flexibility of sensor spacing [1].

Acoustic source localization is done mainly by using DOA, Time of Arrival (TOA), Intensity or Time Difference of Arrival (TDOA) information. Using DOA, we can localize the target by taking each DOA obtained from sensors, and drawing a line of bearing (LOB) [2] from the source to the receiver. The intersection of at least two LOBs will give the source location. This scheme does not require clock synchronization. Intensity-based [3, 4] source localization is motivated by a simple observation that the

sound level decreases when the distance between the sound source and the listener increases. By modeling the relation between sound level (energy) and distance from the sound source, one may estimate the source location using multiple energy readings at different known sensor locations. An implicit advantage of this method is its simplicity: only acoustic energy measured during a specific period is needed. However, this simplicity also implies many practical difficulties that need to be mitigated. In particular, the sensor gain calibration and SNR estimation are two key factors that affect the accuracy of this method. TOA based position estimation is a method which uses time information i.e., the time required for a source signal to the sensors [5]-[7]. Here, multiple spatially separated sensors localize a source by the method of triangulation [8]. The three-dimensional position of a source can be estimated by using three spheres, and each measurement corresponds to the equation of a sphere. The position is estimated by the intersection of these three spheres using TOA measurements [5]-[7]. But in general, direct TOA results in two problems. First, TOA requires that all sources and sensors in the system have precisely synchronized clocks [7]. Second, the source signal must be labeled with a timestamp to allow the sensor to determine the time at which the signal was initiated from the source [7]. This additional time stamp either increases the complexity of the source signal or may not be present in practical scenarios, and may lead to an additional source of error. By using hydrophones we can localize the source by the TDOA based on the intersection of hyperbolic curves [9,10,11]. In TDOA based estimation, a number of spatially separated hydrophones receive the signal transmitted by the source, which needs to be localized.

This paper presents various simulation studies on localization accuracy comparison using AVS and hydrophone based sonobuoys deployed in equal numbers. Section 2 of the paper presents the signal propagation model, section 3 of the paper discusses the methodology used in the determination of position using AVS and hydrophone based sonobuoys. Section 4 discusses the simulation setup and presents the results of various simulation experiments done in the respective sub-sections. Section 5 concludes the study with a summary of the comparison study between hydrophone and AVS based sonobuoys.

2. SIGNAL PROPOGATION MODEL

Let $s(t)$ be the signal and SL be the power of signal in $dBre1\mu Pa$ radiated by the target. PR is the power received in $dBre1\mu Pa$. Also, the power received in Watts is denoted by P_R after including Transmission Loss (TL) at a distance of r m from the source is obtained assuming spherical spreading. The power received is given as:

$$PR = SL - TL$$
$$PR = 171.5 + 20 \log P_R$$
$$PR = 10^{\frac{PR-1715}{20}} W \tag{1}$$

The radiated signal is assumed to be of low frequency so we have not considered absorption loss which is negligible as compared to geometrical spreading loss. The signal received at the ith sensor can thus be expressed as,

$$u_i(t) = \sqrt{(P_R)} * s(t) + n_i(t) \tag{2}$$

Where $n_i(t) \sim N(0, \sigma_i)$ is colored Gaussian noise.

3. METHODOLOGY

In this section, we present the method to find the TDOA and DOA and using them to localize the target.

3.1. Localization by using Time Difference of Arrival (TDOA)

Source localization using TDOA is a two-step process. First, we determine the TDOA of the target between pairs of hydrophones, and then using the TDOA information we localize the target. The sub-section below describes the two-step process.

3.1.1. TDOA estimation using GCC-PHAT

Knapp and Carter [11] provide a description of generalized cross-correlation (GCC) based TDOA estimation method. In particular, the GCC-Phase Transform (GCC-PHAT) method of TDOA does not suffer the spreading of correlation function that other estimation techniques do and hence can provide good performance under reasonable noise conditions. The required mathematical formulation for the GCC-PHAT technique is presented below.

Consider a signal $s_1(t)$ emanating from a source, received under noise at two spatially separated hydrophones as,

$$
\begin{aligned}
u_i(t) &= s_1(t) + n_1(t) \\
u_2(t) &= as_1(t+D) + n_2(t)
\end{aligned}
$$
(3)

Where $s_1(t)$, $n_1(t)$ and $n_2(t)$ are real, jointly stationary random processes, and α is a scaling constant. The signal $s_1(t)$ is assumed to be uncorrelated with noise $n_1(t)$ and $n_2(t)$. Our aim is to estimate the TDOA between the two signals, D. One common method of determining the time delay D is to compute the cross-correlation (CC) function as,

$$
R_{u_1 u_2}(\tau) = E(u_1(t)u_2(t-\tau)]
$$
(4)

Where $E[.]$ stands for expectation operator. The argument τ that maximizes (4) provides an estimate of the delay D. In case of low SNR at the receiver this method fails to estimate the accurate time delay D due to the presence of multiple peaks. GCC is a generalized form of cross-correlation which has received considerable attention due to its ability to avoid spreading of the correlation peak. GCC-PHAT can be mathematically expressed as:

$$
GPHAT = \frac{G_{u_1 u_2}(f)}{|G_{u_1 u_2}(f)|} = e^{j\theta(f)} = e^{j2\pi f D}
$$
(5)

Where $G_{u1u2}(f)$ is the cross power spectral density of u_1 and u_2. Taking the inverse transform of the above equation,

$$
R^{(p)}_{y_1 y_2}(\tau) = \delta(t-D) = F^{-1}(GPHAT)
$$
(6)

Once the TDOAs are estimated, the next step is to estimate the position of the source using the TDOAs. In the subsequent section, we describe a non-iterative approach to estimate the position of a source using TDOAs [12].

3.1.2. Position estimation using TDOA

In this sub-section, we explain the technique used for estimating the source position using TDOAs [12]. Assume there are M sensors distributed arbitrarily in a 2D-plane as shown in fig.1.
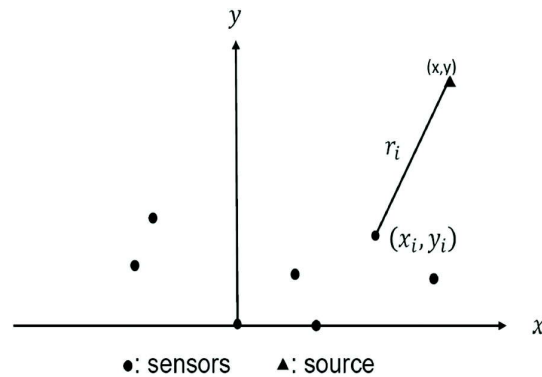

Fig. 1. Localization in 2-D plane.

Now consider the signal $u_i(t)$ received from the source at the ith hydrophone,

$$u_i(t) = s(t - t_i) + n_i(t), \; i = 1,2,...., M \tag{7}$$

where, $s(t)$ is the signal radiating from the source, t_i is the time delay associated with receiver i and $n_i(t)$ is the additive noise at receiver i. The signal and noise are assumed to be mutually independent, zero mean stationary random processes. In order to localize the source, first estimate the TDOA of the signal received at hydrophones i and j using GCC-PHAT. We estimate the TDOA of the signals received at all the sensors with respect to the first sensor *i.e.*, at $i = 1$. TDOAs with respect to the first sensor can be written as,

$$t_{i,1} = t_i - t_1, \; i = 2,3,...., M \tag{8}$$

Let $t_d = [t_{2,1}, \, t_{3,1}, \, ..., \, t_{M,1}]^T$ be the estimated TDOA vector. As shown in fig. 1, the unknown source position is *(x, y)* and the known sensor positions are $(x_i, \, y_i)$. The squared distance between the source and sensor i is

$$r_i^2 = (x_i - x)^2 + (y_i - y)^2$$
$$K_i - 2x_i x - 2y_i y + x^2 + y^2, \; i = 1, \, 2,...., M \tag{9}$$

where, $K_i = x_i^2 + y_i^2$. If   is the propagation speed of the signal, then,

$$r_{i,1} = ct_{i,1} = r_i - r_1, \; i = 1, \, ..., M \tag{10}$$

define a set of nonlinear simultaneous equations whose solution gives *(x, y)*. First, transform these equations into another set of equations. From (10), $r_i^2 = (r_{i,1} + r_1)^2$ so that (9) can be rewritten as,

$$r_{i,1}^2 + 2r_{i,1}r_1 + r_1^2 = K_i - 2x_i x - 2y_i y + x^2 + y^2 \tag{11}$$

Subtracting (9) at $i = 1$ from (11), we obtain

$$r_{i,1}^2 + 2r_{i,1} = -2x_{i,1}x - 2y_{i,1}y + K_i - K_1 \tag{12}$$

where the symbols $x_{i,1}$ and $y_{i,1}$ stand for $x_i - x_1$ and $y_i - y_1$ respectively. It is important to note that the set of equations in (12) is still a nonlinear set of simultaneous equations with unknowns x, y and r_1. To solve for x, y, eliminate r_1 from (14) and produce (M-2) linear equations in x and y. The source position is then estimated using least squares (LS).

Now, we describe a technique proposed in [12] to solve these equations when the number of sensors $M \geq 4$. In this particular case, the system of equations is over-determined as the number of measurements are greater than the number of unknowns. Let $z_a = [z_p^T, r_1]^T$ be the unknown vector, where $z_p = [x, y]^T$. Usually, in the presence of noise, the set of nonlinear equations in (14) will not meet at the same point. Thus, the error vector derived from (14) is,

$$\Psi = h - G_a z_a^0 \tag{13}$$

where

$$h = \frac{1}{2}\begin{bmatrix} r_{2,1}^2 & - K_2 & + K_1 \\ r_{3,1}^2 & - K_2 & + K_1 \\ & ... & \\ r_{M,1}^2 & - K_M & + K_1 \end{bmatrix}$$

$$G_a = -\begin{bmatrix} x_{2,1} & y_{2,1} & r_{2,1} \\ x_{3,1} & y_{3,1} & r_{3,1} \\ . & . & . \\ x_{M,1} & y_{M,1} & r_{M,1} \end{bmatrix} \tag{14}$$

As in presence of noise, there will be an error in TDOAs *i.e.* $t_{i,1} = t_{i,1}^0 + n_{i,1}$, where $n_{i,1}$ is the error in TDOA, and $\{*\}^0$ denotes the noise free value of $\{*\}$. Then, (10) can be used to express the estimated range as,

$$r_{i,1} = r_{i,1}^0 + c n_{i,1} \tag{15}$$

Noting from (10) that $r_i^0 = r_{i,1}^0 + r_1^0$, ψ is found to be

$$\psi = cBn + 0.5c^2 n \odot n$$
$$B = diag\left\{r_2^0, r_3^0, ..., r_M^0\right\} \tag{16}$$

where $\odot$ represents the Schur product (element-by-element product). In practice, the condition $c n_{i,1} << r_1^0$ is usually satisfied. Ignoring the second term on the right of (13), ψ becomes a Gaussian random vector with covariance matrix given by,

$$\psi = E[\psi\psi^T] = c^2 BQB \tag{17}$$

The elements of z_a in (13) are related through $K_i = x_i^2 + y_i^2$, which means that (13) is still a set of nonlinear simultaneous equations in two variables *x* and *y*. The approach to solve this problem is to first assume that there is no relationship among *x, y* and r_1. They can then be solved by the (LS) method. The final solution is obtained by imposing the known relationship $K_i = x_i^2 + y_i^2$ to the computed result via another LS computation. This two-step procedure is an approximation of a true ML estimator for source location. By considering the elements of z_a to be independent, the ML estimate of z_a can be obtained as,

$$z_a = \arg\min\{(h - G_a z_a)^T \psi^{-1}(h - G_a z_a)\}$$
$$= (G_a^T \psi^{-1} Ga)^{-1} G_a^T \psi^{-1} h \tag{18}$$

This is readily recognized as the generalized LS solution of (13). The covariance matrix ψ is not known in practice, as the matrix *B* contains the true distances between source and sensors. Thus, further approximation is necessary in order to make the problem solvable. When the source is far from the array, each r_i^0 is close to r^0 so that $B \approx r^0 I$, where r^0 designates the range and *I* is an identity matrix of size *M*–1. Since, scaling ψ does not affect the answer, an approximation of (18) is,

$$z_a \approx (G_a^T Q^{-1} G_a)^{-1} G_a^T Q^{-1} h \tag{19}$$

If on the other hand source is close, we can first use (19) to obtain an initial solution to estimate *B*. The final answer is then computed using (18). However, (18) can be iterated to provide an even better answer.

3.2. Localization using Direction of Arrival

Localization using DOA is a two-step process. First we determine the DOA of the target and then using DOA information we localize the target. In the sub-section below, we describe the two-step process one by one.

3.2.1. DOA Estimation using Arc Tangent

Let the signal intercepted by the omnidirectional sensors be $u_0(t)$ and the components of the received signal received by two orthogonally placed directional sensors be designated as $u_s(t)$ and $u_c(t)$ where, the subscripts *o, s* and *c*, represent the omni, cosine and sine components respectively[13,14].

$$\begin{bmatrix} u_0(t) \\ u_c(t) \\ u_s(t) \end{bmatrix} = \begin{bmatrix} 1 \\ \cos(\theta) \\ \sin(\theta) \end{bmatrix} * s(t) + \begin{bmatrix} n_0(t) \\ n_c(t) \\ n_s(t) \end{bmatrix} \tag{20}$$

where *s(t)* in (20) is the radiated signal, θ is the incidence angle and $n_0(t)$, $n_s(t)$, $n_c(t)$ are zero mean colored Gaussian noise. Taking the Fourier transform of the above equation,

$$\begin{bmatrix} u_0 \\ u_c \\ u_s \end{bmatrix} = \begin{bmatrix} 1 \\ \cos(\theta) \\ \sin(\theta) \end{bmatrix} * S + \begin{bmatrix} N_0 \\ N_c \\ N_s \end{bmatrix} \tag{21}$$

The bearing estimate $\hat{\theta}$ is expressed as:

$$\hat{\theta} = arctan\left(\frac{\hat{s}}{\hat{c}}\right) \tag{22}$$

where $\hat{S}$ and $\hat{C}$ are defined as

$$\hat{S} = \mathrm{Re}(U_s * U_0^*)$$
$$\hat{C} = \mathrm{Re}(U_c * U_0^*) \tag{23}$$

3.2.2. Position estimation using DOA

A grid-based (GB) method is analyzed as given in [15,16], to solve the single source localization problem. This method is an alternative formulation of the non-linear LS (NLS) estimator, which tries to alleviate the major weaknesses of that approach, namely the need for a good initial point to ensure the estimator does not converge to any local minimum, and the computational burden of the minimization procedure. Our approach is based on making the search space discrete by constructing a grid of N points over the area of interest, and then finding the grid point whose DOAs most closely match the estimated DOA. This approach is much more computationally efficient without losing any accuracy, particularly in the multiple source case. A matrix of MxN is formed as follows,

$$\psi = \begin{bmatrix} \psi_{1,1} & \psi_{1,2} & \cdots & \psi_{1,n} & \psi_{1,N} \\ \psi_{2,1} & \psi_{2,2} & \cdots & \psi_{2,n} & \psi_{2,N} \\ \vdots & \vdots & \cdots & \vdots & \vdots \\ \psi_{1,1} & \psi_{1,2} & \cdots & \psi_{1,n} & \psi_{1,N} \\ \vdots & \vdots & \cdots & \vdots & \vdots \\ \psi_{M,1} & \psi_{M,2} & \cdots & \psi_{M,n} & \psi_{M,N} \end{bmatrix} \tag{24}$$

Where $\psi_{m,n}$ in (24) is the DOA from the mth sensor to the nth grid point. The nth column of ψ is formed from the M DOAs to the nth grid point. The index of the grid point whose DOAs best match the estimated DOAs is evaluated as

$$n* = argmin_n \sum_{n=1}^{N} \left| A(\hat{\theta}_n, \psi_{m,n}) \right|^2) \tag{25}$$

Where $A(X, Y)$ is the angular distance function defined in [14]. The source position is given as the coordinates of then* grid point.
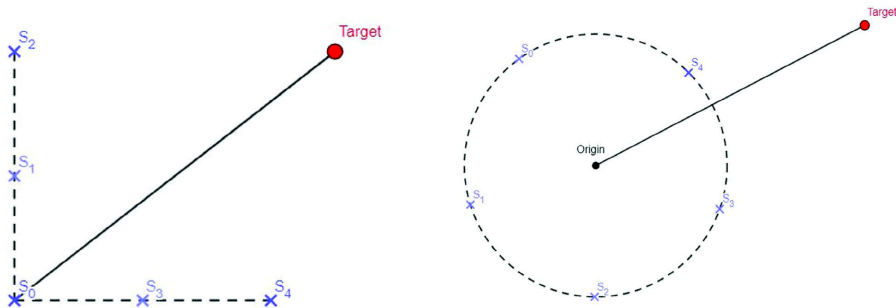
Fig. 2. Sonobuoy placement in L-shape and circular shape.

4. SIMULATION METHOD

The source and sonobuoy placements are shown in Figure 2. Each sonobuoy is equipped with either an omni-directional hydrophone or an AVS. The sonobuoys are deployed in L-shape or circular geometry in this study. The transmitted signal is taken as a narrowband tonal signal of 1second duration which suffers from transmission loss and addition of colored Gaussian noise. We have done the localization comparison using deployment of sonobuoys of AVSs or hydrophones by using the simulation parameters shown in Table 1.

Table 1. Simulation parameters used

S.No	Simulation parameter	Value/Type
1	Radiated signal power level	170 dBre1microPa
2	Sea-state	3
3	Range	1000 and 2000 (m)
4	Geometry	L and Circular shape
5	No. of Sonobuoys	5, 7
6	Transmitting signal frequency	1000 Hz
7	Sampling frequency	44100 Hz
8	Interference signal frequency	1200 Hz
9	Interference signal power level	140 dBre1microPa
10	Method used for Localization using Hydrophone	TDOA
11	Method used for Localization using AVS	DOA
12	Number of Monte Carlo Simulations	100

5. RESULTS AND DISCUSSION

The comparison of localization accuracy between hydrophone and AVS based sonobuoy deployments have been done in the following sub-sections.

5.1. Varying the distance and direction of radiated source with respect to the origin coordinate of sonobuoys for a single source for circular and L-shape for 5 sonobuoys.

In this sub-section, we study the localization performance in terms of RMSE for hydrophone based sonobuoys and AVS based sonobuoys deployed in either circular or L-shape geometry, for the case of 5 sonobuoys of

Fig. 3. RMSE of location estimation with respect to bearing for range of 1000 and 2000 meters for L-shape using hydrophone or AVS based sonobuoys.

either type. The source range from the origin of the coordinate system as measured from the sonobuoy deployment geometries is varied, as also the direction of the source with respect to the x-axis.

From Figures 3 and 4, we observe that AVS based sonobuoys gives more accurate location estimation of the source as compared to hydrophone based sonobuoys except at few angles for both L shape and circular geometries of deployment. Also, by comparing figures 3 and 4, it is seen that the circular geometry provides significantly larger improvement in localization accuracy as compared to L-shape geometry.
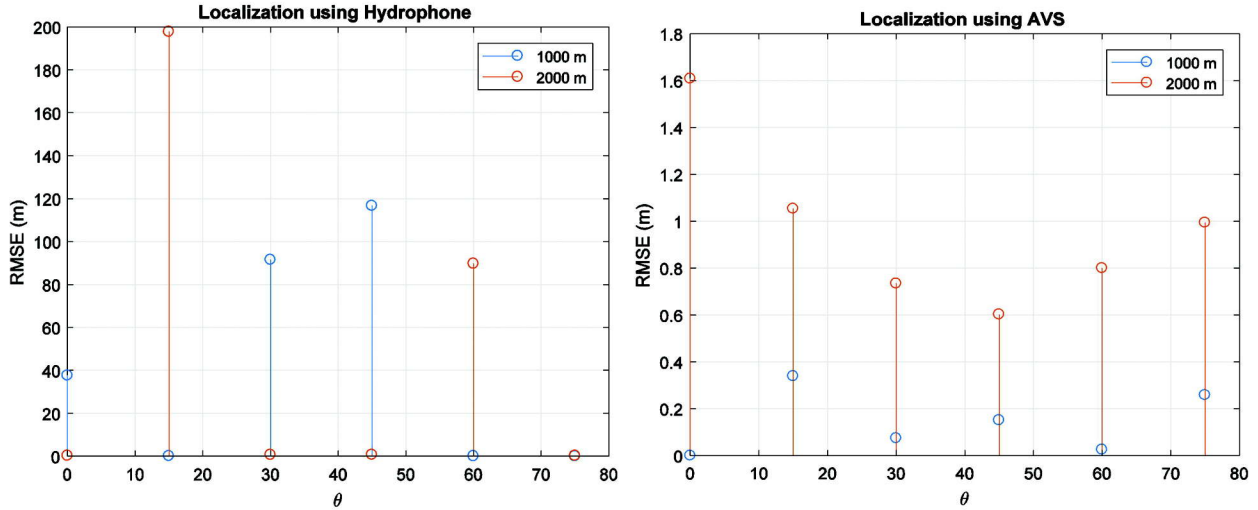
Fig. 4. RMSE of location estimation with respect to bearing angle for range of 1000 and 2000 meters for circular shape geometry using hydrophone or AVS based sonobuoys.

5.2. Varying the distance and direction of radiated source with respect to the origin coordinate of sonobuoys for a single source for circular and L-shape for 7 sonobuoys.

Similar to the observations for 5 sensor geometries in the previous sub-section, it can be observed from Figures 5 and 6, that AVS based sonobuoys gives more accurate location estimation of the source as compared to hydrophone based sonobuoys except at few angles for both L-shape and circular geometries of sonobuoy
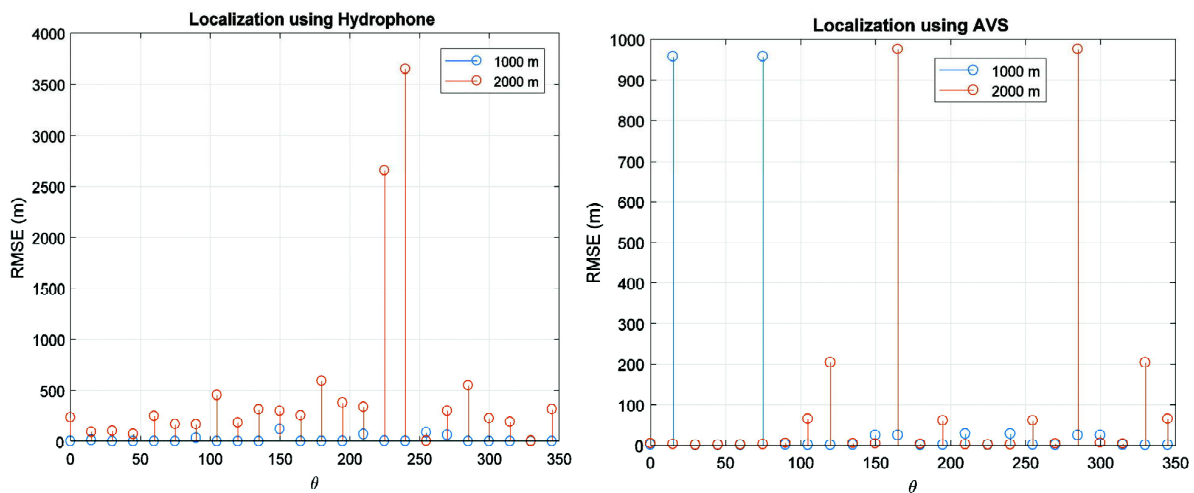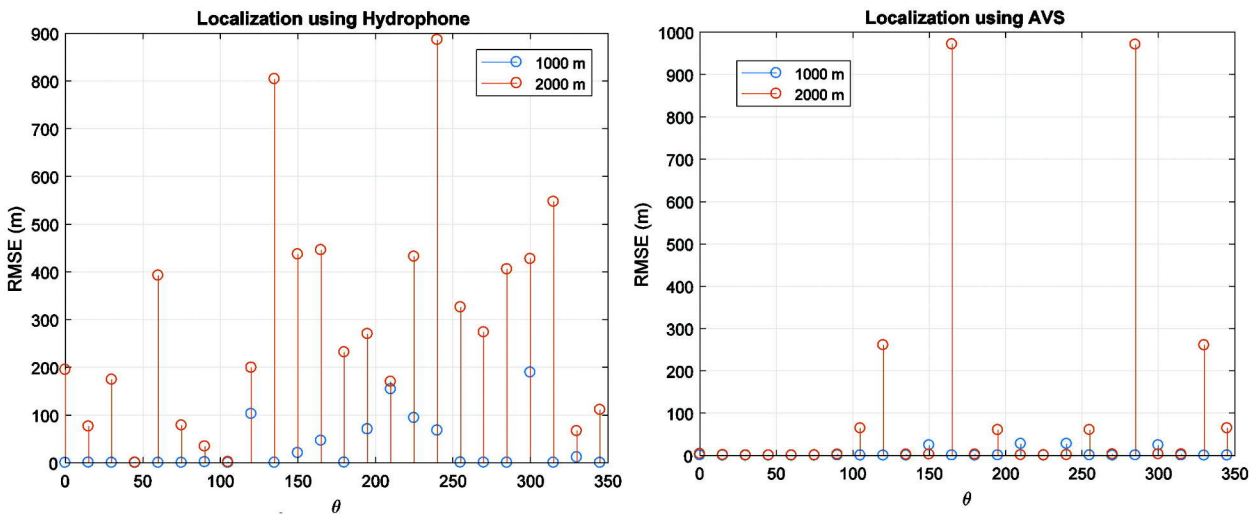

Fig. 5. RMSE of location estimation with respect to bearing for range of 1000 and 2000 meters for L-shape using hydrophone or AVS based sonobuoys.
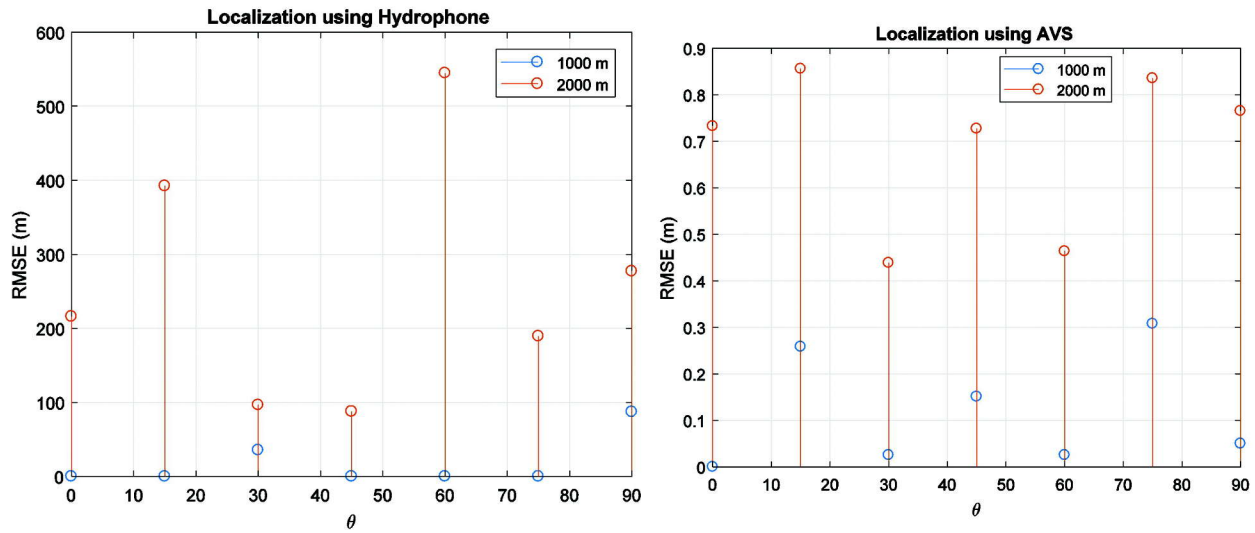
Fig. 6. RMSE of location estimation with respect to bearing for range of 1000 and 2000 meters for circular shape using hydrophone or AVS based sonobuoys.

system deployment. Also, by increasing the number of sonobuoys from 5 to 7 for both hydrophone and AVS based systems, the localization accuracy is improved.

5.3. Varying the distance between sonobuoys in addition to varying the distance between radiated source with respect to the origin coordinate of sonobuoys for L-shape geometry of deployment

In this sub-section, we report the simulation study on the deployment distance between the sonobuoys, for both AVS and hydrophone types. In Figure 7, we can observe that the RMSE decreases on increasing the distance between sonobuoys from 100 m to 400 m. Also, AVS based sonobuoys gives more accuracy as compared to hydrophone based sonobuoys. In Figure 8, we can see that as the mean distance between the sonobuoys and target increases with increase in the number of sonobuoys, there is an increase in the RMSE. Hence, it can be inferred from this study that the mean distance between sonobuoys and target directly affects the RMSE.
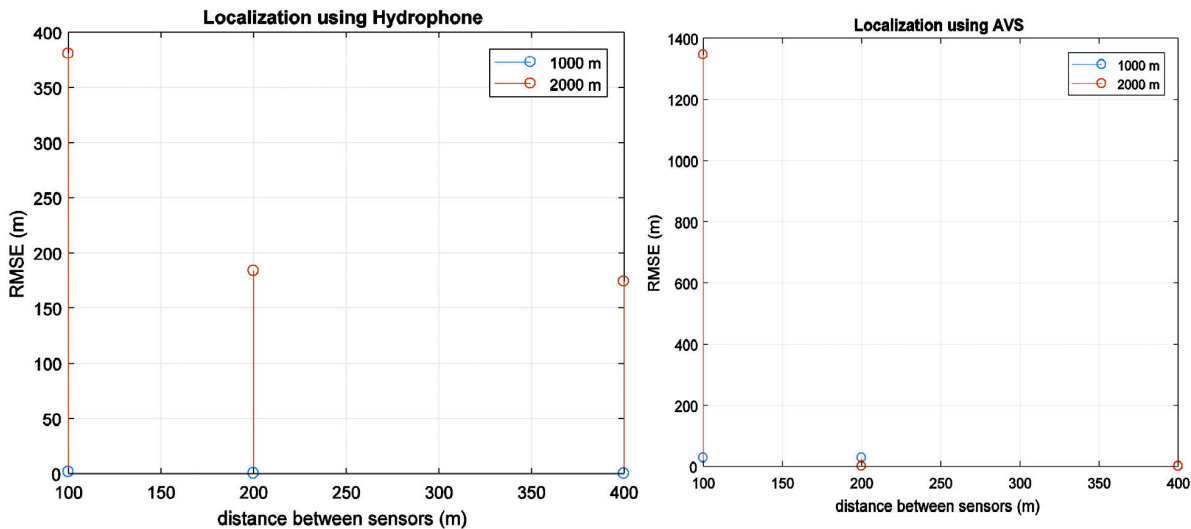
Fig. 7. RMSE of location estimation with respect to distance between sonobuoys, for range of 1000 and 2000 meters for L-shape using hydrophone or AVS based sonobuoys.
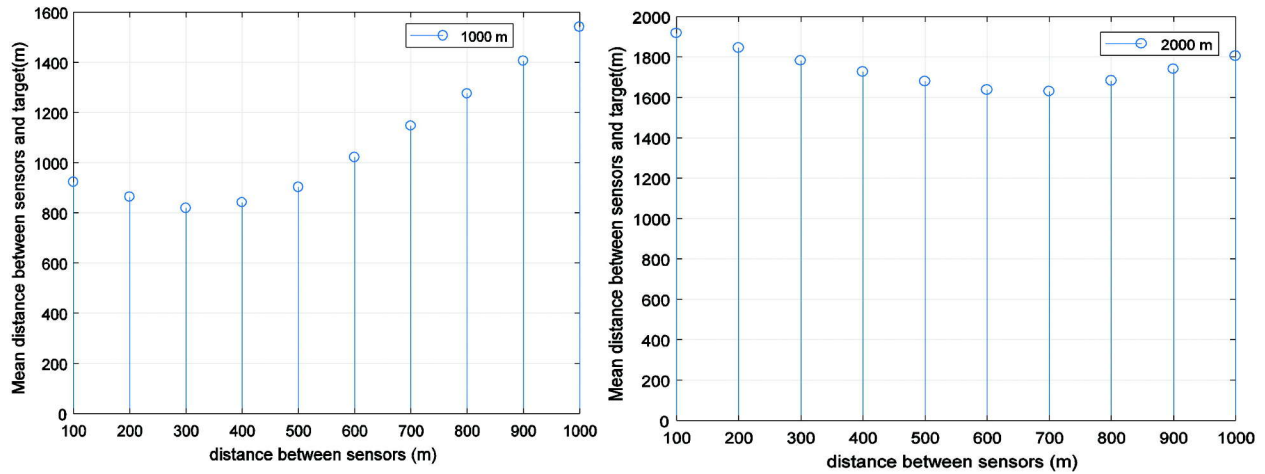
Fig. 8. Mean distance between sonobuoys and target
when the target is at (i) 1000 m, and
(ii) 2000 m from the origin coordinate of the sonobuoys.

5.4. Varying the SNR of single source with respect to the origin coordinate of sonobuoys for circular and L-shape deployment geometries with 5 sensors.

In this sub-section, we consider the performance as a function of the SNR of the source that is measured with respect to the origin coordinate of the sonobuoys. From Figures 9 and 10, we can see that RMSE of localization using either hydrophones or AVS based sonobuoys decreases with increase in SNR except at SNR =20 dB using hydrophone for L-shape geometry due to increase in mean distance. It is also seen that L-shape and circular geometry provide about the same RMSE.
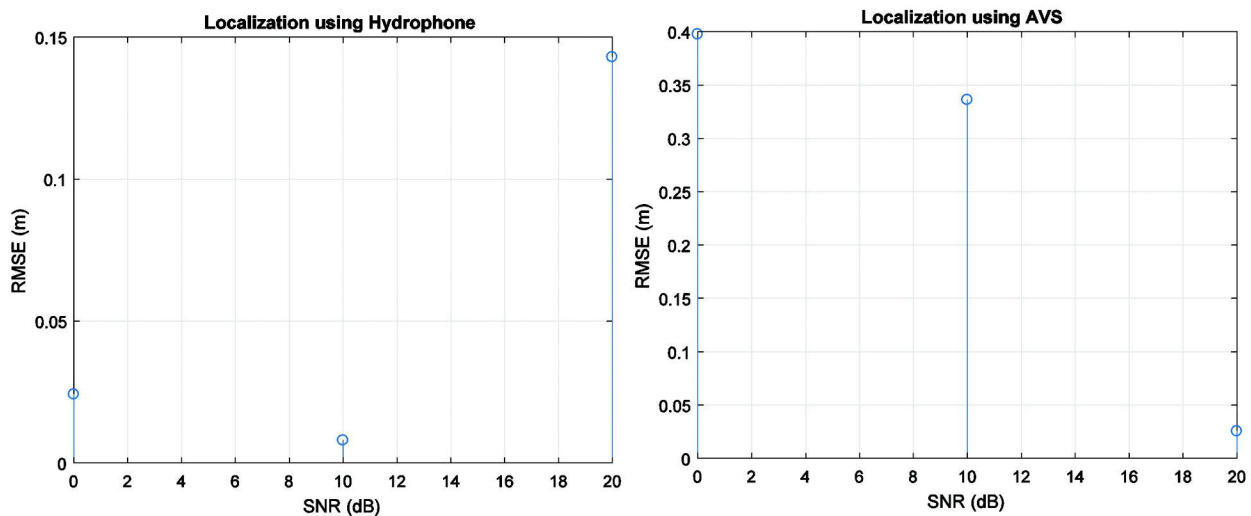
Fig. 9. RMSE with respect to SNR for sea-state 3 and
L-shape using hydrophone or AVS based sonobuoys.
Target is located at 30 degrees to the x-axis.
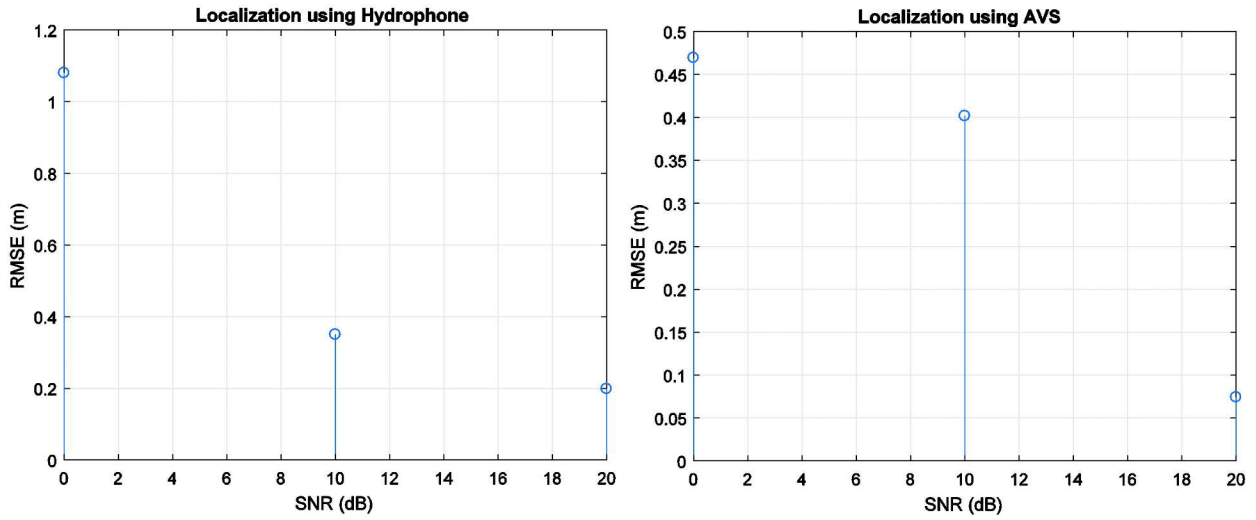
Fig. 10. RMSE with respect to SNR for sea-state 3 and circular shape using hydrophone or AVS based sonobuoys. Target is located at 30 degrees to the x-axis.

5.5. Varying the SNR of single source with respect to the origin coordinate of sonobuoys of a single source for circular and L-shape with 7 sensors.

Here, we show the analysis of RMSE performance as a function of the SNR of the source signal as measured at the origin of the deployed sonobuoy system. From Figures 11 and 12, it is seen that RMSE of localization using either hydrophone or AVS based sonobuoys both decrease with increase in SNR, except at SNR = 20 dB SNR for L-shape hydrophone sonobuoy system deployment. On increasing the number of sonobuoys from 5 to 7, both the geometries provide similar values of RMSE.
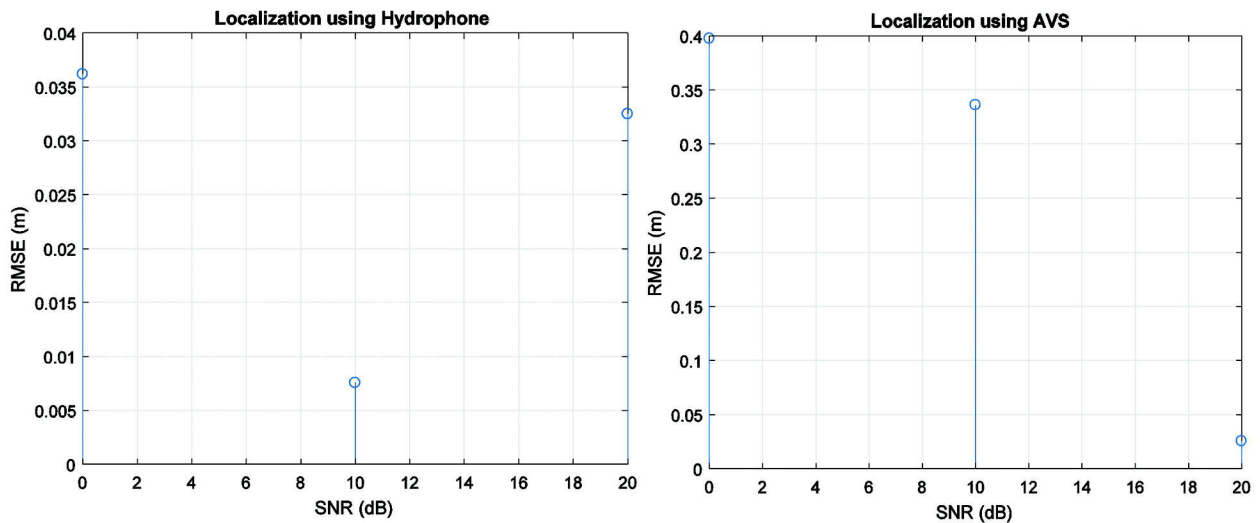
Fig. 11. RMSE with respect to SNR for sea-state 3 and L- shape using hydrophone and AVS based sonobuoys.
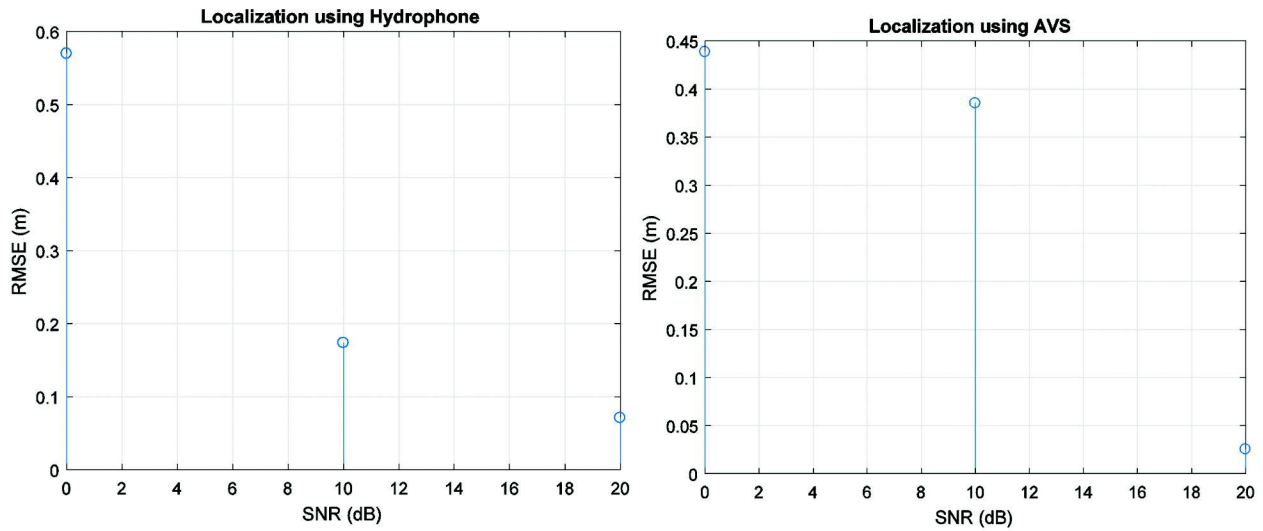
Fig. 12. RMSE with respect to SNR for sea-state 3 and circular shape using
hydrophone and AVS based sonobuoys.

5.6. Varying the distance and direction of radiated source with respect to the origin coordinate of sonobuoys in the presence of multiple sources for 7 sensors.

In this study, we have varied the interference source angle with respect to x-axis and have kept the target position fixed at (i) 1000 m and (ii) 2000 m, with an angle of 30 degrees from the x-axis. From Figures 13 and 14 we can observe that the AVS based sonobuoys gives much better accuracy as compared to hydrophone based sonobuoys. Also, it can be observed that the circular geometry does not provide significant improvement in localization accuracy as compared to L-shape geometry in the presence of interference source.
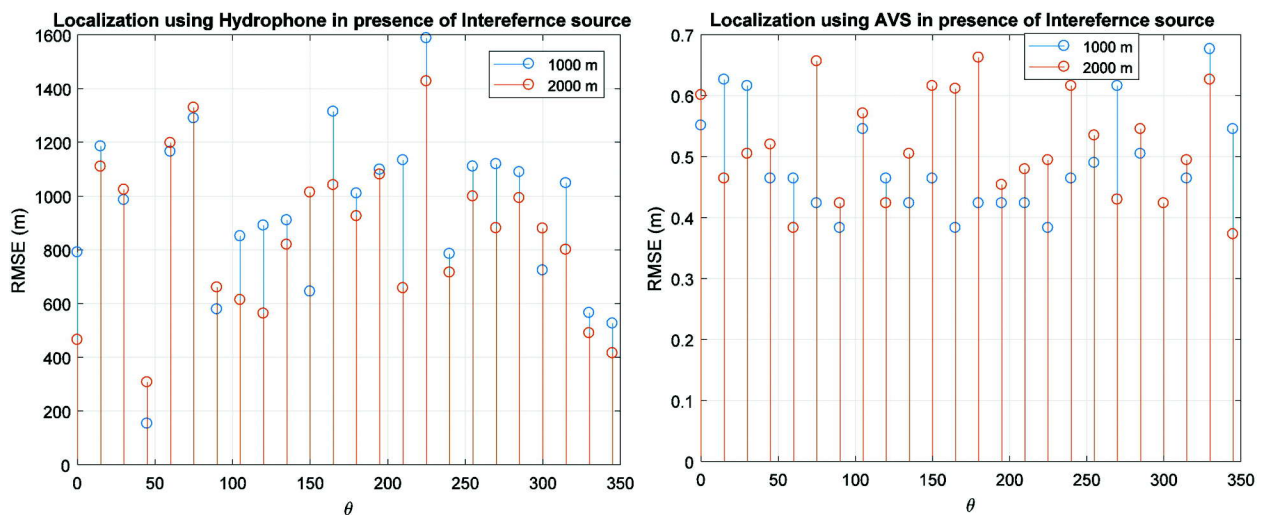
Fig. 13. RMSE of source localization with respect to bearing angle for sea-state
3 and L-shape using hydrophone and AVS based sonobuoys in the
presence of interference source.
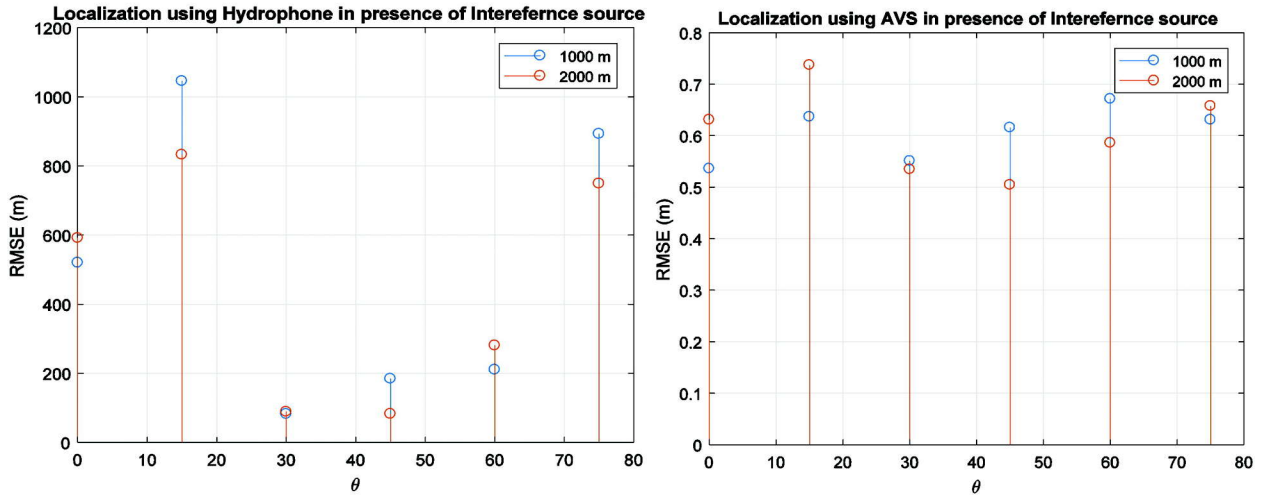
Fig. 14. RMSE of source localization with respect to bearing angle for sea-state 3and circular shape using hydrophone and AVS in presence of interference source.

5.7. Varying the distance and direction of single source with respect to the origin coordinate of sonobuoys in the presence of random drift of 50 m.

In this sub-section, we study the localization performance in terms of RMSE for hydrophone based sonobuoys and AVS based sonobuoys deployed in either circular or L-shape geometry in addition to random drift in sensors with standard deviation of 50 m, for the case of 7 sonobuoys of either type. The source range from the origin of the coordinate system as measured from the sonobuoy deployment geometries is varied, as also the direction of the source with respect to the x-axis.
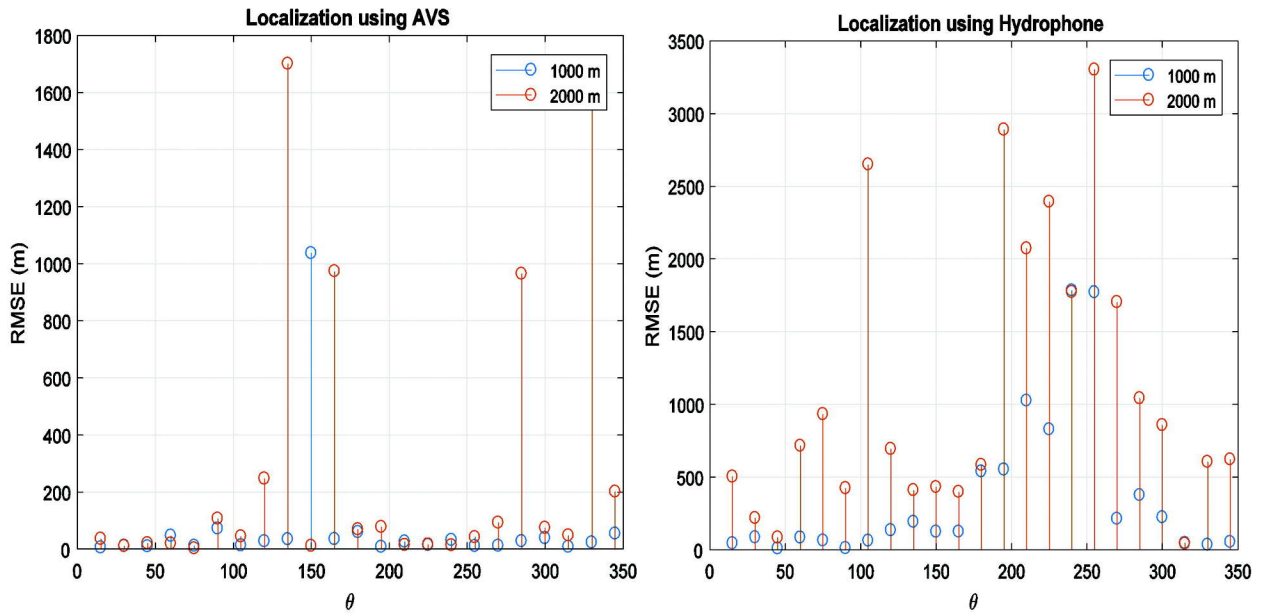
Fig. 15. RMSE of source localization with respect to bearing angle for sea-state 3 and L-shape using hydrophone and AVS based sonobuoys inin the presence of random drift of sensor positions of 50 m standard deviation.
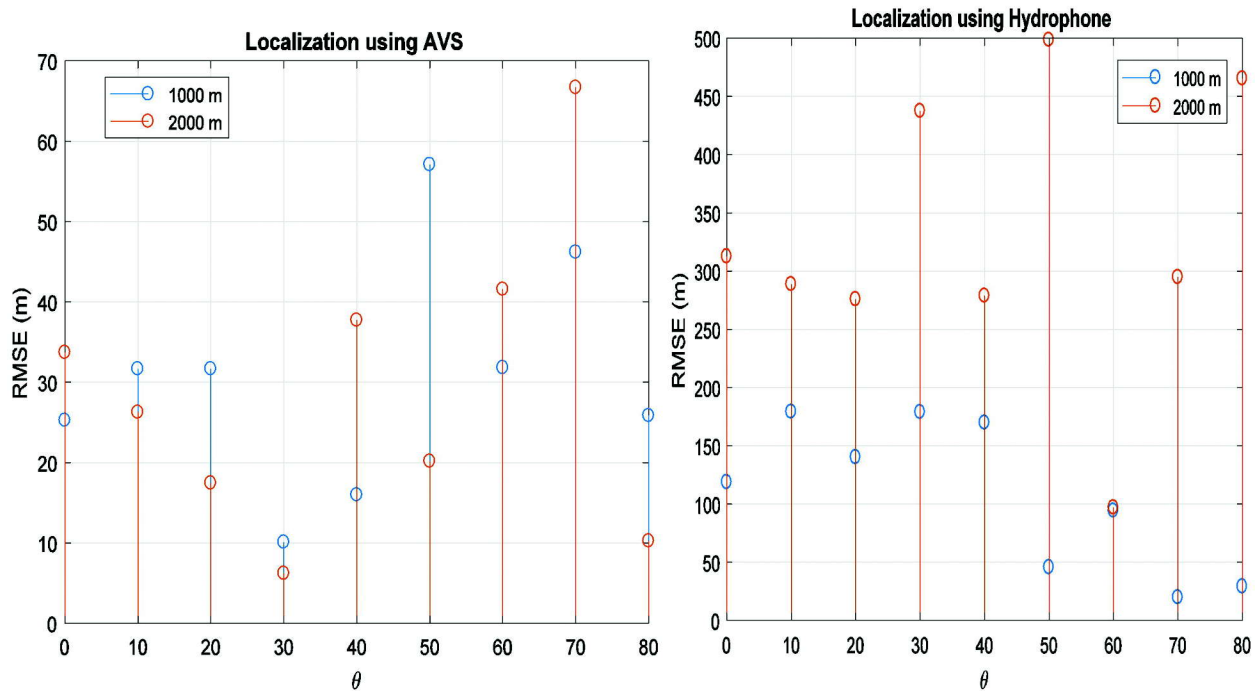
Fig. 16. RMSE of source localization with respect to bearing angle for sea-state 3and circular shape using hydrophone and AVS in presence of random drift of sensor position of 50 m standard deviation.

From Figures 15 and 16, we observe that AVS based sonobuoys gives more accurate location estimation of the source as compared to hydrophone based sonobuoys except at few angles for both L- shape and circular geometries of deployment. Also, by comparing Figures 15 and 16, it is seen that the circular geometry provides significantly larger improvement in localization accuracy as compared to L-shape geometry.

6. CONCLUSION

We have first discussed methods from the literature to estimate TDOA and DOA using GCC-PHAT and arc-tangent algorithms respectively. These methods are applicable for the hydrophone based sonobuoys and the AVS based sonobuoys respectively, since a single omnidirectional hydrophone does not provide DOA information. Based on the estimated TDOA and DOA, we have presented methods to localize the target in 2-D space. For comparing localization using AVS or hydrophone based sonobuoys, several simulation studies have been done to examine the various dependencies of localization performance. The main observations are (i) a circular geometry provides better accuracy as compared to L-shape geometry of sonobuoy deployment, (ii) increasing the number of sonobuoys improves the localization accuracy, and iii) AVS based sonobuoys provide better localization accuracy as compared to hydrophone based sonobuoys, especially in the presence of an interference source. The paper also gives quantitative values of the improvement in terms of RMSE localization errors for various cases that may be useful in planning practical deployment strategies for sonobuoy based source localization.

7. REFERENCES

[1]   A. Nehorai and E. Paldi, 1994. "Acoustic vector-sensor array processing," *IEEE Trans. Signal Process,* **42**, 2481-2491.

[2]   J. Reed, C. da Silva and R. Buehrer, 2008. "Multiple-source localization using line-of-bearing measurements: Approaches to the data association problem," *Proc. IEEE Military Communications Conference,* pp. 1-7.

[3]   X. Sheng and Y.H. Hu, 2005. Maximum likelihood multiple-source localization using acoustic energy measurements with wireless sensor network. *IEEE Trans. Signal Process*, **53**, 44-53.

[4]   D. Li and Y. Hu, 2003. Energy-based collaborative source localization using acoustic microsensor array. *EURASIP J. Appl. Signal Process,* pp. 321-327.

[5]   B.T. Fang, 1990. "Simple solutions for hyperbolic and related position fixes," *IEEE Transactions on Aerospace and Electronic Systems,* **26**(5), 748-753.

[6]   J. Abel and J. Smith, 1987. "The spherical interpolation method for closed-form passive source localization using range difference measurements," Acoustics, Speech and Signal Processing, *IEEE ICASSP '87*, pp. 471-474.

[7]   T.S. Rappaport, J.H. Reed and B.D. Woerner, 1996. "Position location using wireless communications on highways of the future," *IEEE Communications Magazine,* **34**(10), 33-41.

[8]   M. Vossiek, L. Wiebking, P. Gulden, J. Wieghardt, C. Hoffmann and P. Heide, 2003. "Wireless local positioning," *IEEE Microwave Magazine,* **4**(4), 77-86.

[9]   G. Carter, 1981. "Time delay estimation for passive sonar signal processing," *IEEE Transactions on Acoustics, Speech, and Signal Processing*, **29**(3), 463-470.

[10]   W. Hahn and S. Tretter, 1973. "Optimum processing for delay-vector estimation in passive signal arrays," *IEEE Transactions on Information Theory,* **19**(5), 608-614.

[11]   C. Knapp and G. Carter, 1976. "The generalized correlation method for estimation of time delay," *IEEE Transactions on Acoustics, Speech, and Signal Processing,* **24**(4), 320-327.

[12]   Y.T. Chan and K.C. Ho, 1994. "A simple and efficient estimator for hyperbolic location," *IEEE Transactions on Signal Processing,* **42**(8), 1905-1915.

[13]   S. Davies, 1987. "Bearing accuracies for arctan processing of crossed dipole arrays," *Proc. Oceans Conference,* pp. 351-356.

[14]   B.H. Maranda 2003., "The statistical accuracy of an arctangent bearing estimator," *Proc. Oceans Conference,* **4**, 2127-2132.

[15]   A. Griffin and A. Mouchtaris, 2013. 'Localizing multiple audio sources from DOA estimates in a wireless acoustic sensor network', *Proc. IEEE Workshop on Applications of Signal Processing to Audio and Acoustics,* pp. 1-4.

[16]   A. Griffin, A. Alexandridis, D. Pavlidi, Y. Mastorakis and A. Mouchtaris, 2015. A.: 'Localizing multiple audio sources in a wireless acoustic sensor network', *Signal Processing,* pp. 54-67.

Acoustic imaging and prospecting with back propagation in time reversal based on discrete huygens' modelling, Revisited

Y. Kagawa[1], Y. Zhao[1], L. Chai[1], N. Wakatsuki[1] and M. Singh[2]
[1]Department of Electronics and Information Systems, Akita Prefectural University,
Tsuchiya-Ebinokuchi 84-4, Yurihonjo, Akita 015-0055, Japan
[2]Acoustics and Vibration Metrology Section
CSIR-National Physical Laboratory, Dr. K.S. Krishnan Marg, New Delhi-110 012, India
[1]y2kagawa@gmail.com, [2]mahavir.acoustics@gmail.com

ABSTRACT

The paper discusses the discrete Huygens' modelling to describe the propagation and the application to the acoustic imaging, demonstrated with the back propagation in time reversal process. Discrete Huygens' model is a discrete version of the Huygens' Principle, with which the sequence and the process of the progress and the scattering can be simulated for wave propagation phenomena. As it provides a physical model, it does not require the solution of the wave equation but traces the sequences of the impulse scattering at the nodes taken at the intersections in the orthogonal transmission-line models. The advantage of the present physical model lies on the fact that as the algorithm is absolutely stable and as the inverse scattering matrix is the same as the original forward one, the same algorithm applies to the back propagation in time reversal due to the system in symmetrical with respect to time. The energy distribution evaluation over the field of interest leads to the imaging of an object under sensing.

1. INTRODUCTION

Imaging, exploration and prospecting are important fields in remote sensing. Acoustic waves have been used for sensing for many decades.

The most popular pulse echo sounding is a radar-type imaging technique, in which the imaging is made due to the strength of the reflected pulse and its transmission time to the reflected pulse from an object surface. The emanating wave must have a narrow beam, which is to be steered. The advantage of this system is that the pulse wave transmitting and receiving can be made one-sidedly, while the disadvantage is that the imaging is disturbed by the presence of the irregular field in the paths through which the emanating and reflected waves travel. Since the invention of so-called X-ray CT, the transmission type imaging systems of various kinds have been developed. An object to be sensed is placed between the transmitter and the receiver, between which the attenuation is measured along a line. The measurement is repeated as the direction of the line of the measurement is rotated. The image is reconstructed from the data back projected[1]. The narrow beam is again required, and the scattering and reflection at the various media intersurfaces are a nuisance and may cause an error. Another imaging technique is a scattering

tomography. Born or Rytov approximation must be used for linearizing the wave equation. It does not always work reasonably in practice[2].

The imaging technique in the present paper belongs to the scattering tomography but depends on the different mechanism, based on the back propagation in time reversal. For the image reconstruction, the back propagation uses the same algorithm as the forward propagation. The imaging lays in the fact that the scattered signals come back to the original source points from the secondary sources, that is, the reflection between the object surface and the surrounding medium.

The imaging techniques are an inverse problem. Some mathematics of the solution in time reversal process has been discussed. A wave equation is reversely solved, that is, initial conditions and parameters are sought from the response data for the wave equation and the associated boundary conditions[3]. A mirror process could be associated[4]. It is not easy to solve and not straightforward.

The present approach is based on the completely different mechanism as that no wave equation needs be solved inversely. Instead, the spatial energy density distribution is only evaluated in association with the backpropagation process. The region of higher pressure density corresponds to the secondary source regions that include the sources from the inner surfaces boundaries.

The paper first introduces the discrete Huygens' models, developing the scattering matrix for the medium of different impedances.

It is also shown that the inversion of the scattering matrix leads to the original scattering matrix, not only for the standard matrix regardless of the modified matrix for different propagation velocity and density. This is an alternative proof of the reciprocity principle and the system symmetry for time. In next physical problems, the systems are symmetrical with time, at least in ideal sense. The more example of simulation based on the back propagation in time reversal are demonstrated for the cases when all the data are accessible on the remote surface surrounding an object and for some cases when some data are missing, as the prospecting must sometimes be required on the one-sided boundary.

2. PROPAGATION

2.1 Discrete Huygens' models

The present paper first introduces a discrete counterpart to the Huygens' principle[5] - [10]. Some explanations are repeated for the paper to be self-contained.

The discrete Huygens' modelling which the authors refer to is known as the transmission-line matrix modelling (TLM) in the electromagnetic engineering community, which is best explained by the equivalent electrical transmission-line theory. P. B. Johns originally developed it for the electromagnetic field problem analysis [11] - [13].

What is particular about his method is that the solution is sought in a transmission-line network equivalently taken to the field of interest in the time domain, while the transmission-line has traditionally been solved in the frequency domain. The time domain solution is then obtained by Laplace transformation. The time domain solution procedure is here made for a series of the equally spaced transmission lines, which results in the scattering of the impulses at the crossed nodes taken at the equally spaced intervals. As computers become increasingly powerful both in execution time and memory size, engineers sometimes favour the direct time-domain approach, which provides the full wave solution.

We consider here the sound wave propagation and confine ourselves to a two-dimensional field model. As the sound wave is scalar, generality will not be lost because of the two-dimensional modelling. It is very easy to extend to the three-dimensional modelling except that it requires more computational resources. Waves radiate from a point source spherically. According to Huygens' principle, a wavefront consists of some secondary point sources, each of which gives rise to spherical waves, and the envelope of these waves forms a new spherical wavefront which again gives rise to a new generation of spherical waves and so on. The Huygens' principle is here considered in the discrete sense to implement this process of sequences

on a digital computer. This process is assumed to occur adhering to the directions of the Cartesian coordinates. The propagation takes place as the sequence of the impulse transmission and scattering at a node or an element with four to six branches of the transmission lines. When a sound impulse of unit amplitude is incident to one of the nodes, the sound impulses scatter in four to six directions.
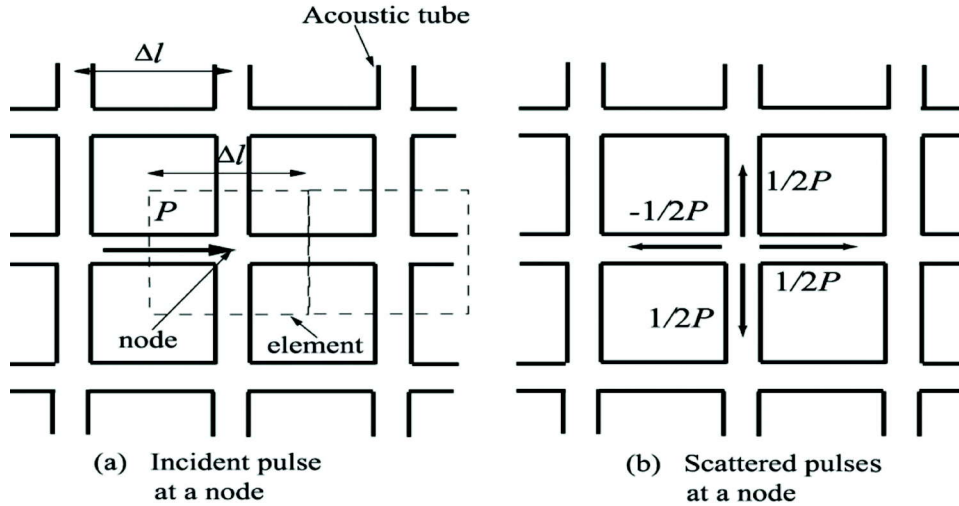
Fig. 1. Discrete Huygens' model for the acoustic tube mesh corresponding to the field

A two-dimensional acoustic field is equivalently placed by the orthogonal mesh made of the acoustic transmission lines or tubes as shown in Fig. 1. The orthogonally connected transmission lines form impedance discontinuity at the node because the characteristic impedance in a tube (= $\rho c_0 S$, where ρ is density and c_0 sound speed and S cross-sectional area) is the same for each branch and three branches are connected to one at the node, so that the impedance looked from one branch into the node is one-third. When an impulse of amplitude P is incident to one of the nodes, the scattering takes place. Each scattered pulse has one-quarter of the incident energy, and the magnitude of the scattered pressure is one-half, in which the sign of the reflected one to the incident direction is negative. This resembles the collision of the elastic balls of molecules as shown in Fig. 2 (a).
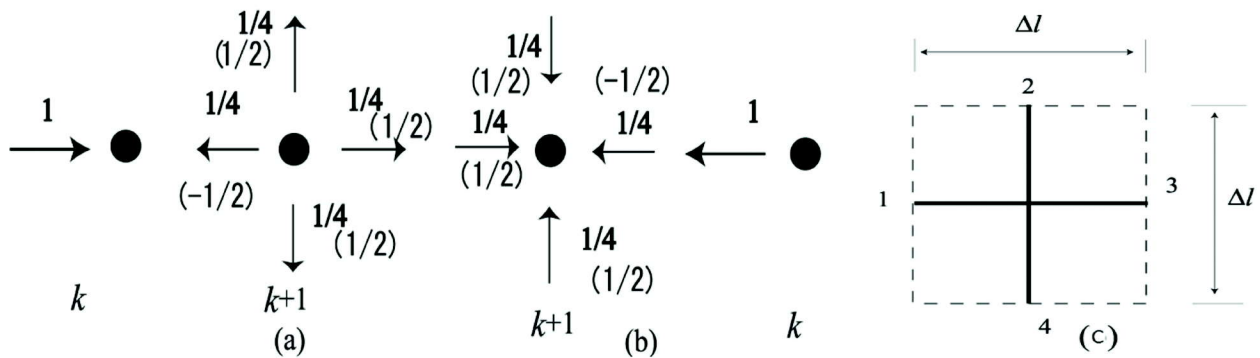
Fig. 2. Scattering and concentration in a two-dimensional element.
(a) Incident and scattered impulses; (b) time-reversed process. Numbers indicate the amount of energy (those in the parenthesis are for pressure); (c) the branches are numbered in clockwise.

For the general case, four impulses $P^1 \sim P^4$ are incident to the four branches at the same time $t = k\Delta t$ (where $\Delta t = \Delta_0 l / c_0$ is the time delay required for a pulse to travel the distance Δl, c_0 is propagation speed

along the tube or in free field, and k is the integer). The response can be obtained by superposing the contribution from all branches. The scattered impulse S^n at branch n at time $t + \Delta t = (k + 1)\, \Delta t$ is given as

$$_{k+1}S^n = \frac{1}{2}\sum_{m=1}^{4} {}_k P^m - {}_k P^n \tag{1}$$

where, $_k P^n$ indicates the incident impulse at branch n at time $t = k\Delta t$. This can be rewritten in the form of a scattering matrix expression as

$$\begin{bmatrix} S^1 \\ S^2 \\ S^3 \\ S^4 \end{bmatrix}_{k+1} = \frac{1}{2}\begin{bmatrix} -1 & 1 & 1 & 1 \\ 1 & -1 & 1 & 1 \\ 1 & 1 & -1 & 1 \\ 1 & 1 & 1 & -1 \end{bmatrix}\begin{bmatrix} P^1 \\ P^2 \\ P^3 \\ P^4 \end{bmatrix}_k$$

or
$$_{k+1}\{S\} = [A]\ {}_k\{P\} \tag{2}$$

where *[A]* is can be called a scattering matrix. Pressure $P_{i,j}$ at the node of an element is given by

The radiated signal is assumed to be of low frequency so we have not considered absorption loss which is negligible as compared to geometrical spreading loss. The signal received at the ith sensor can thus be expressed as,

$$P_{i,j} = \frac{1}{2}\sum_{n=1}^{4} {}_k P^n \tag{3}$$

where, subscripts *i, j* represent the nodal position *(x, y) = (iΔl, jΔl)*, and the superscript numbers are referred to Fig. 2(c).

When the field is divided into square meshes, the scattered pulses which travel along the branches in reverse directions become incident pulses to the adjacent elements at whose nodes scattering again takes place. The scattered pulses represent the incident pulses to a node at position *(i, j)* at the adjacent nodes as

$$_{k+1}P^1_{i,j} = {}_{k+1}S^3_{i-1,j}, \qquad _{k+1}P^1_{i,j} = {}_{k+1}S^1_{i-1,j}$$
$$_{k+1}P^2_{i,j} = {}_{k+1}S^3_{i,j+1}, \qquad _{k+1}P^4_{i,j} = {}_{k+1}S^2_{i,j-1} \tag{4}$$

This is the compatibility condition for the element connection. Repeating the operation of equations (2)-(4) on all nodes, the impulse responses in the field are traced at successive time intervals. The method is inherently the time domain approach, which is quite suitable for the simulation and visualisation of wave propagation behaviour on the computer.

2.2 Wave equation

It is possible to show that the wave equation can be created from the scattering algorithm.

Eq. (1) is substituted into Eq. (3) and applying the compatibility condition (4) in consideration of the adjacent nodes, so that the following expression is obtained for the pressures

$$_k P_{i-1,j} + {}_k P_{i+1,j} + {}_k P_{i,j-1} + {}_k P_{i,j+1} - 4\, {}_k P_{i,j} = 2({}_{k-1}P_{i,j} - 2\, {}_k P_{i,j} + {}_{k+1}P_{i,j}) \tag{5}$$

This expression leads to the wave equation as the distance Δl becomes small. This means that the discrete Huygens' model is equivalent to FD-TD, but it should be emphasised that the algorithm or the solution process is quite another. What is important is that the present model provides a physical model following to the Huygens' principle, which does not require the numerical solution of the wave equation, and present process is absolutely stable.

Expansion of Eq. (5) in Tayer series about $_k P_{i,j}$ arrives at the wave equation

$$\frac{\partial^2 P}{\partial x^2} + \frac{\partial^2 P}{\partial y^2} = \frac{1}{c^2}\frac{\partial^2 P}{\partial t^2} + \varepsilon \tag{6}$$

with small error term ε, where

$$\varepsilon = 2\left\{\frac{\Delta l^2}{4!}\left(\frac{\partial^4 P}{\partial x^4} + \frac{\partial^4 P}{\partial y^4}\right) + \frac{\Delta l^4}{6!}\left(\frac{\partial^6 P}{\partial x^6} + \frac{\partial^6 P}{\partial y^6}\right) + \cdots\cdots\right\} + 4\left\{\frac{1}{4!}\frac{\partial^4 P}{\partial t^4} + \frac{\Delta l^2}{6!}\frac{\partial^6 P}{\partial t^6} + \cdots\cdots\right\}$$

which vanishes as $\Delta l \to 0$. As for Eq. (5) is valid for any $_kP_{i,j}$, it is replaced by P and $c = c_o/\sqrt{2}$.

Two routes or schemes are possible for computer simulation, as shown in the followings.

Numerical model

Wave equation ⟷ FD-TD

Wave propagation

Computer simulation

Huygens' principle ⟷ Scattering algorithm

Physical model
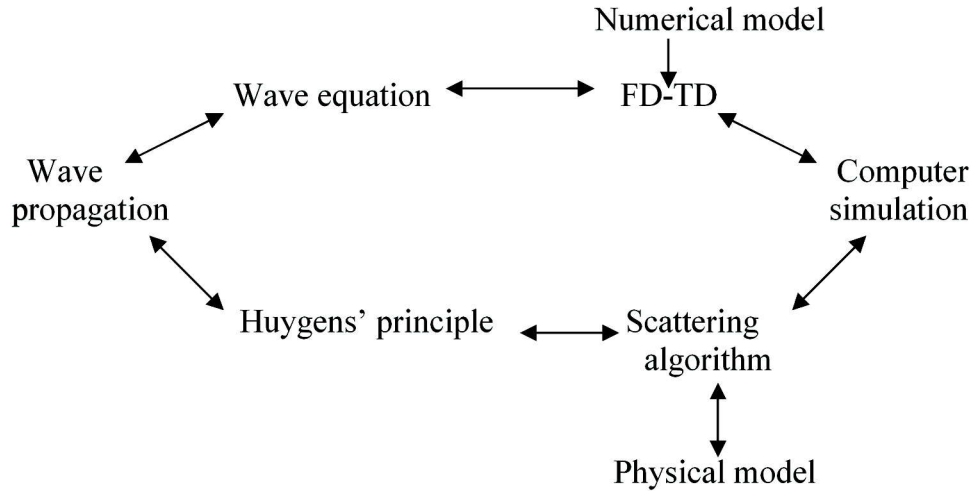
2.3 Propagation

By comparing Eq. (6) with the wave equation in free field, one finds that period the propagation speed in our network is slower by the factor $1/\sqrt{2}$ than that of the free field $c_0\sqrt{2}$ is a fraction, which corresponds to the diagonal length of the mesh. This factor is $1/\sqrt{3}$ for the three-dimensional field modelling. The propagation speed along the line is also delayed due to the presence of a pair of stubs of length $\Delta l/2$ attached to a rode. The propagation velocity C_p one transmission lines in x - or y-direction is given by

$$C_p = C_0 \frac{\pi sl}{\lambda \sin-1\left\{\sqrt{2}\sin\left(\frac{\pi sl}{x}\right)\right\}}$$

$$\approx \frac{1}{\sqrt{2}} \quad for\ small\ \lambda \tag{7}$$

The line shows a low-pass characteristic, having the cut-off at $\Delta l = \lambda/4$.

The propagation on speed depends on the direction of the propagation, and cause the dispersion effect, which is not very large as $C_p/C_o = 0.981$ for $\Delta l/\lambda = 1/10$. Please see the references (13), (16) for more information.

Dispersive systems are not exactly symmetric with time as waves propagate. In many engineering problems, however, the dispersion is supposed to be small so that the effect is involved. The effect may appear in terms of some errors.

2.4 Non-reflective boundary

In many applications, an infinite domain simulation must be required. To achieve this condition, the non-reflective boundary must be provided surrounding the field of interest. The simplest and the most practical

way is to terminate the boundary of the field by the characteristic impedance Z_0 (= ρc_0) of the free field. As in our network field, the travelling speed is lower by the factor $1/\sqrt{2}$, the reflection coefficient at the boundary must be

$$\tau = \frac{Z_0\sqrt{2} - Z_0}{Z_0\sqrt{2} + Z_0} = -0.17157 \tag{8}$$

With this condition imposed on the branch contacting to the outer space, the transparent condition can practically be assumed on the boundary as a quasi-boundary. This is however only valid for the plane wave incidence. The reflection slightly increases for the oblique incidence. Many other modelling is attempted to reduce the reflection. For some models, one assumes that no reflection wave is possible [14] and another provides absorbing multi-layers [15].

2.5 Inhomogeneous and dissipative media

The medium can be inhomogeneous, which can be realised by providing a proper stab tube or transmission line connected to the node as the 5th branch, with which the field characteristic impedance or the propagation speed can be varied (decreased). The stub works as an additional compliance or capacitance with the time synchronisation kept. This is illustrated in Fig. 3.
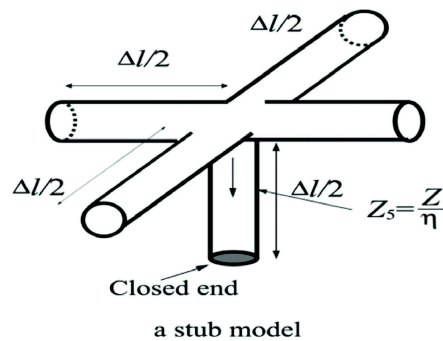
Fig. 3. Stub tube model with the fifth branch (velocity is controlled by the presence of this branch with the characteristic impedance changed by choosing parameter η property)

The scattering matrix defined in Eq. (2) is now given as

$$[A] = \frac{1}{2 + \dfrac{\eta}{2}} \begin{bmatrix} a & 1 & 1 & 1 & \eta \\ 1 & a & 1 & 1 & \eta \\ 1 & 1 & a & 1 & \eta \\ 1 & 1 & 1 & a & \eta \\ 1 & 1 & 1 & 1 & \eta \end{bmatrix} \tag{9}$$

where, η is the characteristic impedance parameter of the stub tube, and

$$a = -\left(1 + \frac{\eta}{2}\right), \quad b = -\left(2 - \frac{\eta}{2}\right)$$

Pressure vectors $_{k+1}\{S\}$ and $_k\{P\}$ consist five components. The condition for the 5th branch is that the input pulse to the 5th branch, is reflected back to the node with time delay Δt from the closed end, which has no connection to other elements so that $_kP5 = {}_{k+1}P5$

Though it is not directly concerned with the present paper, some are commented for other field conditions. The dissipative field can also be modelled by the introduction of another 6th tube of infinite length. The infinite length means no reflection, introducing energy dissipation. The wave propagation in

the mean-flowing medium means that the propagation speed is accelerated or retarded depending on the direction of the flow. This situation can also be incorporated in the modelling by providing the extra arms at one node directionally coupled with adjacent nodes [9].

3. BACK PROPAGATION

3.1 Propagation in time reversal

It is not always a simple task to solve the wave equation inversely, analytically or numerically [4]. The particular feature of the present model is that as it is a physical model, the back propagation in time-reversal is possible and can easily be implemented. Our scattering matrix expression is expressed by

$$_{k+1}\{S\} = [A]_k \ \{P\} \tag{10}$$

Premultiplying $[A]^{-1}$ on both side, knowing that

$$[A]^{-1} = [A] \tag{11}$$

One has thus,

$$_k\{P\} \ = \ [A]_{k+1} \ \{S\} \tag{12}$$

This is a time reversal process. The mechanism is depicted in Fig. 2(b). The mechanism is depicted in Fig. 2(b). It is interesting that identity of Eq. (11) is valid not only for Eq. (2) but also for Eq. (9) so that the backpropagation algorithm is the same as that of the forward propagation without regarding the medium properties. This is our finding in the present paper. The time reversal invariance is also mentioned in the particle model (17). The inversion of Eq. (9) can easily be checked by the use of MATHEMATICA. This means that when the output signals were put back into the places at which signals are measured, they came back to the original input source points. This is the key mechanism that can be utilised for the source identification and tomographic imaging. In the physical problem, systems are symmetrical with time, provided they are ideal. It is not so in real cases, where the loss is present so that the entropy increases as the wave propagates. The systems are, to be exact, not symmetrical with time. In many engineering models, however, when the loss is small, it can be ignored. The effect of the loss is evaluated regarding the errors as such. In the present demonstration here we only consider such cases where the systems are a reversal in time

Suppose an object whose characteristic impedance is different from that of the surrounding medium. When a source illuminates it, scattering will take place from its boundary. The scattered data collected along a line surrounding the field that encloses the object are back-propagated, and then the signals will go back to the source by way of the secondary sources over the object boundary. It suggests a possibility of imaging the presence of the inhomogeneity boundaries in the backpropagation approach by evaluating the energy density distribution in the space.

3.2 Some demonstrations

3.2.1 Source identification

Some identifications were well-demonstrated for the multiple and distributed sources in ref. [10].

The original sound sources are reversed from the scattered data collected by the receiving array along the surrounding boundary. The wave signals are recorded at many points over a surrounding boundary (non-reflective). They are put into the receiving boundary back, and then the waves go back to the source points. The simulated results show that if the data are collected at the interval points apart more than the wavelength of the signals, the identification may fail.

3.2.2 Imaging

The case when the impedance of an object, ρc is higher by 10% (due to higher density) than that of the surrounding medium is demonstrated in ref. [10]. In the present paper, the examination is extended to the cases with the media of different propagation speed and with the different energy evaluation processes of

the data. The object is illuminated by point sources over the boundary enclosing the object, and the scattered data are all recorded which are assumed to be the measured data. In the simulation, that is, the forward propagation responses are used for the 'measured' data. The data signals recorded are back-propagated into the vacant free space. For all the simulation to follow, the one-shot emanation of 16 impulses with the Gaussian profile is used for the exciting sound sources.

For imaging two possible data processing are considered. (Process 1): One procedure is to obtain the spatial distribution of the time-integrated energy at every node of the mesh in the back-propagation process. The spatial distribution is calculated concerning the values distributed for the empty field. (Process 2): Another procedure is that the compensation is made for the 'measured' data concerning the reference data calculated for the empty field before the backpropagation. The compensated data are then back-propagated into the free space for which the time-integrated energy density distribution is evaluated.
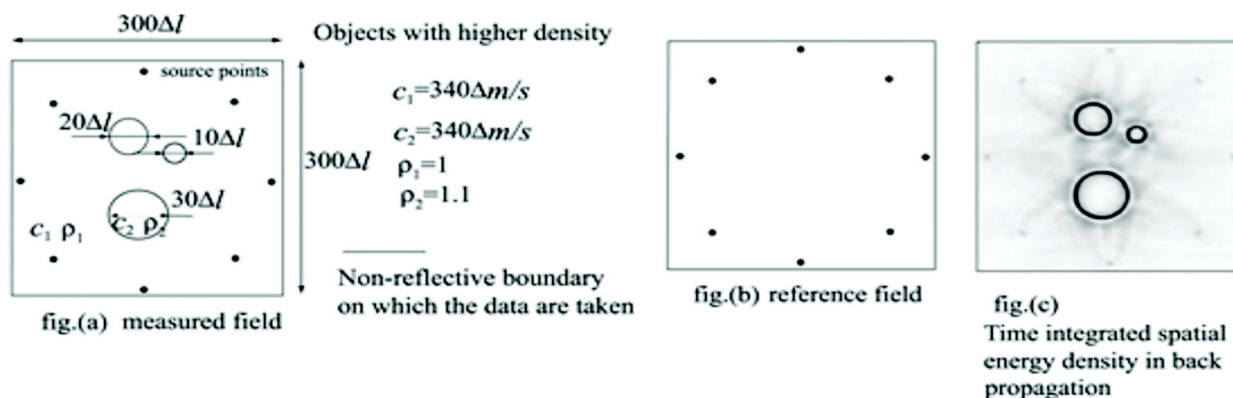
Fig. 4. Inversion, Multi-objects with higher density (Process 1)

Fig. 4 shows the case of multi-body objects when their mass density is 10% higher than that of the surrounding medium, while their propagation velocities are the same. With Process 1, the objects' boundaries are well visualised. However, for the case when the propagation speeds are different while the density is the same (the case when the propagation speed is lower by 10% in the objects), the results are very poor as shown in Fig.5. This last case can be improved with the use of Process 2. The results are as shown in Fig. 6.

The back-propagation is taken for every single excitation, and the result is superposed for all excitations.
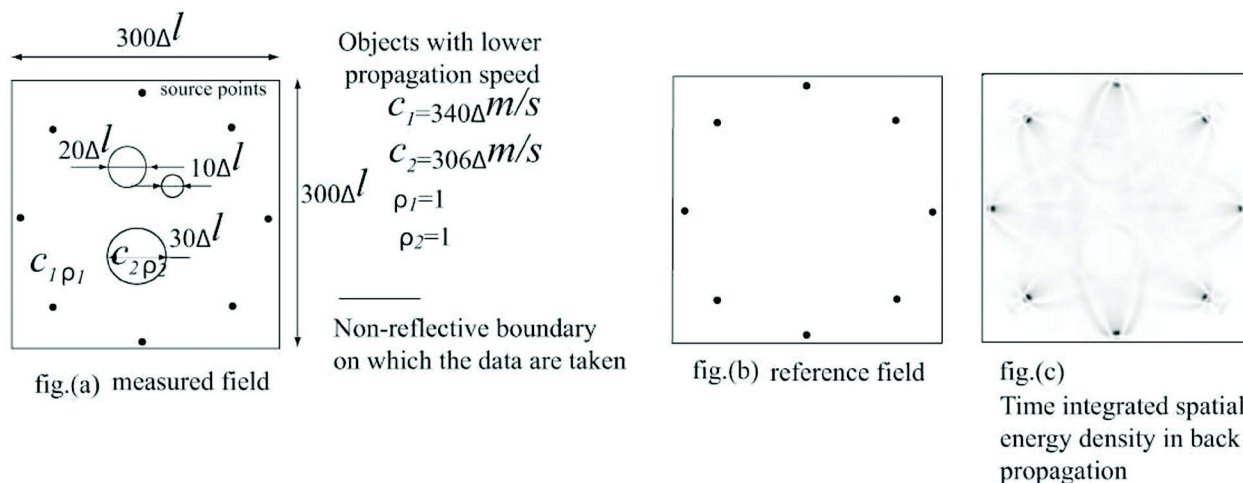
Fig. 5. Inversion, Multi-objects with lower propagation speed (Process1)
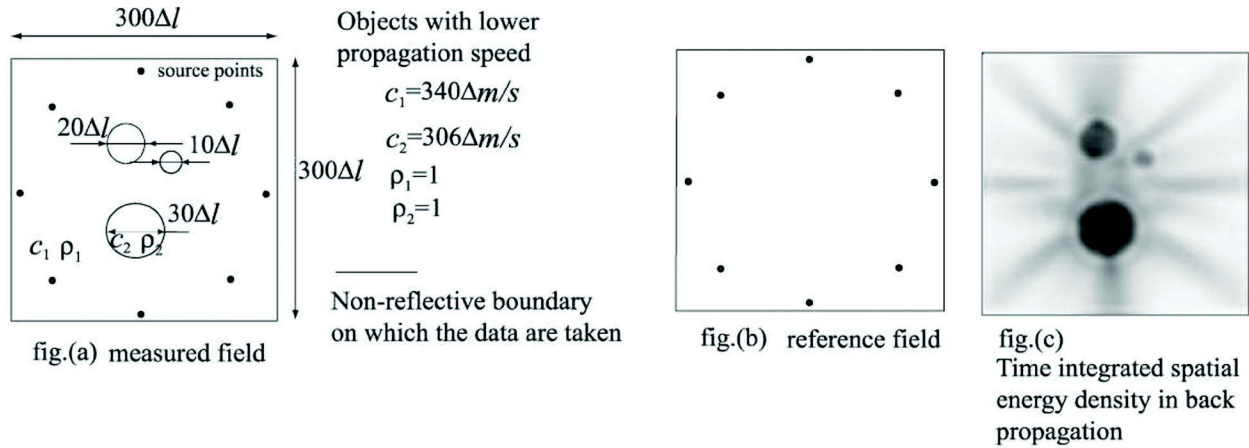
Fig. 6. Inversion, Multi-objects with lower propagation speed (Process 2)

Fig. 7 shows the result when the propagation speed in the objects is higher by 10% (Process 2). The objects are again visible, but their diameters look slightly smaller, while in Fig. 6, the objects look slightly larger. This effect may also happen in a radar-type echo-imaging.
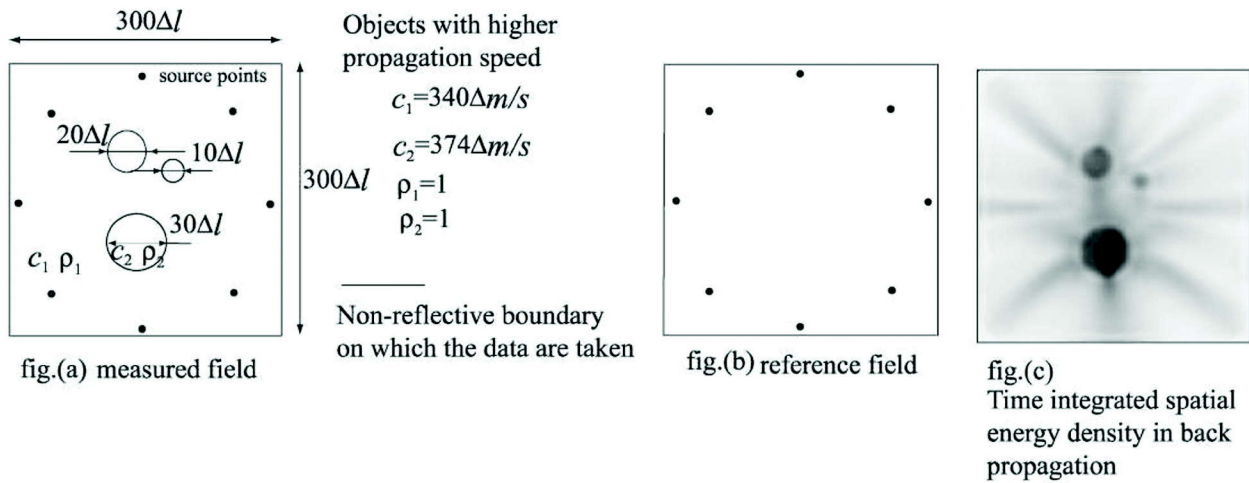
Fig. 7. Inversion, Multi-objects with higher propagation speed (Process 2)

For the field with different propagation velocity, it is found that Process 2 is more effective.

Fig. 8 is the case when the data are not complete, but the hard surface is assumed to present at the bottom which could work as the mirror sources (Process 2). The images are visible.

The back-propagation approach is a scattering tomography. Fig. 8 show that single-sided illumination is possible, but if all received data transmitted from the object are not collected, the result is degraded, as examined in the next simulation.

3.2.3 Sounding

Single-sided sounding models are then considered. Fig. 9 shows an example, in which a circular object with higher impedance (by 10%) is located beneath the ground or sea surface. A point source is provided over the ground surface over which the data are also taken. With different source point, only a part of the upper surface boundary is visible. Fig. 10 is the case when two boreholes driven into the ground are provided for the transmitted data collection. The sound source is placed on the ground surface, and the data are accessible
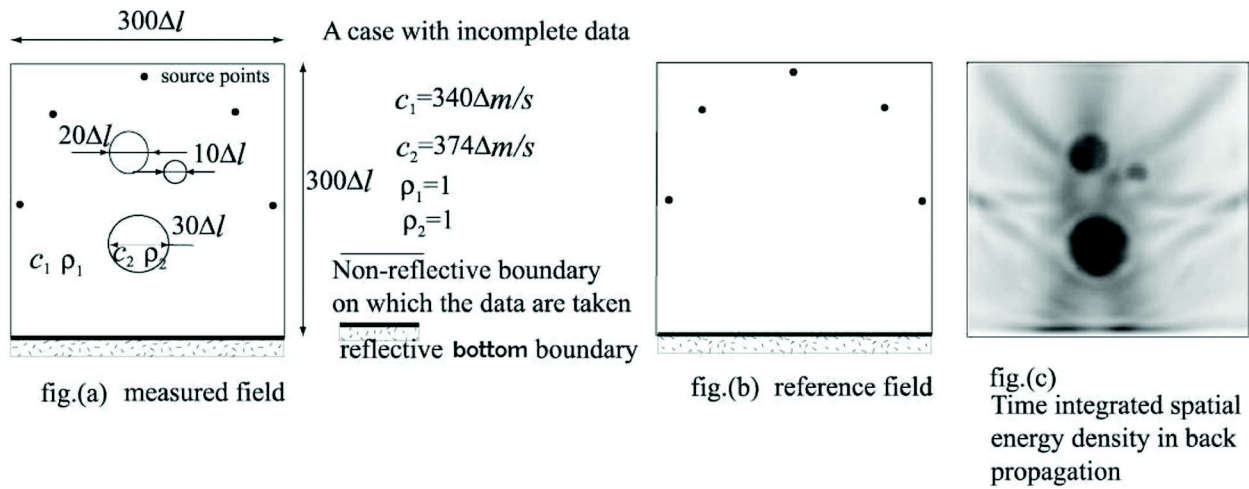
Fig. 8. Inversion, A case with incomplete data
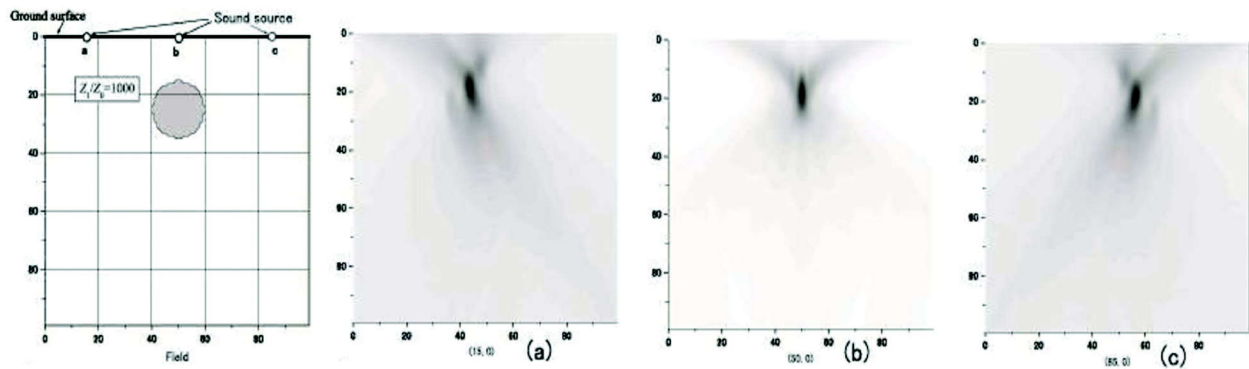
Fig. 9. Inversion, One-sided illumination and data collection
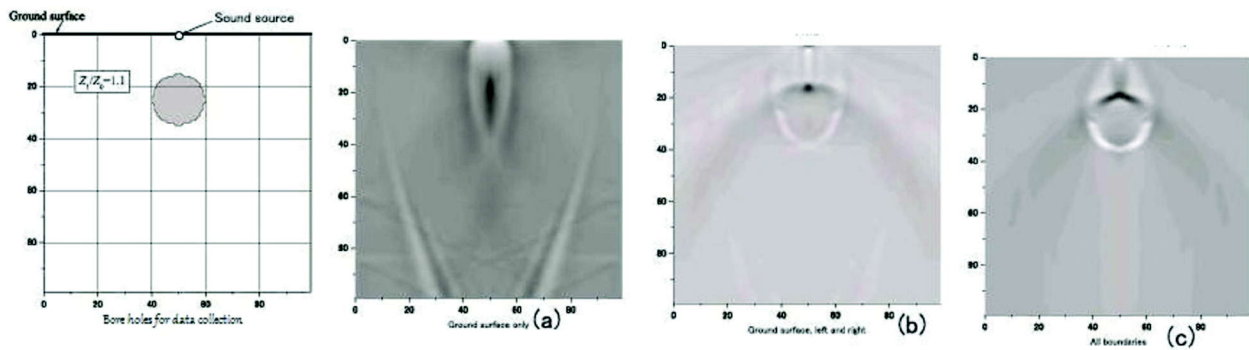
Fig. 10. Sounding with boreholes for data collection

at three-sided boundaries. The result is improved as shown in Fig. (b). Fig. (c) shows the cases when the data could be obtained at the bottom included. In all cases, we see artefacts between the circular objects, which may be caused by the wave interferences.

At this stage, we show the presence of the object boundaries. The quantitative evaluation of the object materials must be our next question.

4. CONCLUDING REMARKS

The discrete Huygens' models have been examined, and the use of the back-propagation approach has been proposed for the imaging. The imaging approach is quite different from that of the so-called scattering tomography. Our finding is that the inversion of the scatting matrix becomes the same matrix without regarding the medium properties. The possibility of the imaging and the remote sensing are here demonstrated by simulation. Extension to the three-dimensional field modelling is straightforward. The present approach features a new technique to the imaging and the remote sensing, which does not require a beam-formed sound source and complex reversal calculation. In the present simulation, we are only concerned about the acoustic wave. The case of the elastic wave problems can also be within our reach[10].

We came across the Viggen's paper of the lattice Boltzmann Method applied to the acoustics based on the particle models. The paper is available via WEB[17] and latest work[18,19]. He introduced the Chopard-Luthi wave model, one of the simplest models among lattice Boltzmann model, which is directly applicable to the wave problems. For comparison, he referred discrete Huygens's model and expressed the interests for the difference. We rather felt the similarity on the contrary, as they take ensemble average for Boolean occupation number, while we take a model of impulsive excitations and responses. This is the motivation of the present paper, where the title accomplishes "revisited".

5. ACKNOWLEDGEMENT

6. REFERENCES

[1] A.C. Kak and M. Slaney, 1988. Principles of Computerized Tomographic Imaging, (New York: IEEE Press).

[2] Y. Kagawa, T. Tsuchiya, T. Ishihara and K. Fujioka, 1996. Some experimental considerations on ultrasonic computed tomography, *Journal of Acoustic Society of Japan,* **52**(8), 605-615.

[3] M.K. Klibanov and A. Timonov, 2003. On the mathematical treatment of time reversal, *Inverse Problems.* **19**, 1299-1318.

[4] M. Fink and C. Prada, 2001. Acoustic time-reversal mirrors, *Inverse Problems*, **17R**, 1-38.

[5] Y. Kagawa, 1997. Computational Acoustics – Theories of Numerical Analysis in Acoustics with Emphasis of Transmission-line Matrix Modeling, Int. Symp. on Simulation, *Visualization and Auralization for Acoustic Research and Education, Tokyo,* pp. 19-26.

[6] Y. Kagawa, 2003. Discrete Huygens' model and its application to acoustics. 10th *Int'l. Congress on Sound & Vibration, Stockholm*, 7-10, July.

[7] Y. Kagawa, T. Tsuchiya, B. Fujii and K. Fujioka, 1998. Discrete Huygens' model approach to sound wave propagation, *J. Sound & Vib.*, **218**(3), 419-444.

[8] Y. Kagawa, T. Tsuchiya, T. Hara and T. Tsujii, 2001. Discrete Huygens' modelling simulation of sound wave propagation in varying velocity environments, *J. Sound & Vibr.* **246**(1), 419-436.

[9] Y. Kagawa, Tsuchiya, K. Fujioka and M. Takeuchi, 1999. Discrete Huygens' model approach to sound wave propagation?reverberation in a room, sound source identification and tomography in time reversal, *J. Sound & Vib.,* **225**(1), 61-78.

[10] Y. Kagawa, T. Fujitani, Y. Fujita, L. Chai, N. Wakatsuki and T. Tsuchiya, 2002. Discrete Huygens' modelling approach to wave propagations in a homogeneous elastic field, *J. Sound & Vib.,* **255**(2), 323-335.

[11] P.B. Johns and R.L. Beurle, 1971. Numerical solution of 2-dimensional scattering problems using a transmission-line matrix, *Procs. Inst. Elec. Eng.,* **118**, 1203-1208.

[12]   P.B. Johns 1974. The solution of inhomogeneous waveguide problems using a transmission-line matrix, *IEEE Trans. Microwave Theory and Techniques, MTT*, **22**, 209-215.

[13]   Y. Kagawa, N. Yoshida, T. Tsuchiya and M. Sato, 2000. Introduction to Equivalent Circuit Network Modelings, (Tokyo: Morikita-Shuppan) (in Japanese).

[14]   J.A. Morente, J.A. Porti and M. Khalladi, 1992. Absorbing boundary conditions for the TLM method, *IEEE Trans. Microwave Theory and Techniques, MTT-* **40**(11), 2095-2099.

[15]   L. Chai, S. Nogi, Y. Kagawa and N. Wakatsuki. 2005. Absorbing boundary conditions in Transmission-line Matrix (TLM) modelling, *J. Japan Society for Simulation Technology,* **24**(1), 59-65.

[16]   C. Christopoulos, 1995. The transmission line modelling method, *IEEE Publications.*

[17]   E.M. Viggen, 2009. The lattice Boltzmann method with application in Acoustics, Thesis, Dept. of Physics -NTNU.

[18]   Renato S.T. de Carvalho, Julio A. Cordioli, 2016. Simulation of underwater acoustics and sediment wave propagation using the Discrete Huygens Modeling (DHM), *Proceedings of Forum Acusticum EAA Conference, Krakow,* pp. 1-8.

[19]   A. Alia, 2018. Application of Discrete Huygens Method for Diffraction of Transient Ultrasonic Field, *Acoustical Physics,* 2018, **64**(1), 10-17.

Acoustic analyses of intonation in two dialects of Kannada - A comparative study

Theaja Kuriakose, Shridevi S Govanakoppa and Sangeetha V
JSS Institute of Speech and Hearing, Kelageri, Near Tapovana,
Sri Shivarathreeshwara Nagar, Dharwad-58007, Karnataka
crz148292@iitd.ac.in

ABSTRACT

Intonation refers to the change of fundamental frequency in a sentence. Intonation helps the speakers to express their ideas or emotions. There have been very limited studies to examine the effect of dialect in Intonation. The present study aimed to investigate and compare the terminal contour of intonation between Bangalore dialect Kannada and Dharwad dialect Kannada in sentences depicting various emotions. The results indicated differences in the intonation pattern between the dialects. The results also indicated presence of compound tone more in Dharwad dialect Kannada compared to Bangalore dialect Kannada.

1. INTRODUCTION

In human communication, prosodic features play an important role. These features make the system of communication productive and accurate. Prosody may reflect various features of the speaker or the utterance: the emotional state of the speaker; the form of the utterance (statement, question, or command); the presence of irony or sarcasm; emphasis, contrast, and focus; or other elements of language that may not be encoded by grammar or choice of vocabulary. The speech will sound monotone, if prosodic aspect of speech is affected. "Although much of the message in speech is conveyed by the segmental phonemes; additional information is carried out by the prosodic features"[1]. "Prosody may serve as the interface between low level segmental information and higher level grammatical structures in speech"[2]. Since, speech is considered as the primary mode of human communication, knowledge of prosodic features is essential to scientifically study the human communication and speech.

Intonation, rhythm and stress are classically understood as prosodic parameters. Intonation refers to the change of fundamental frequency in a sentence. Intonation helps the speakers to express their ideas or emotions .It is usually the terminal F0 pattern which varies across the different sentence types in non-tonal languages [3]. The study of intonation has attracted a great deal of scholarly attention, despite the difficulty in analysing this property of spoken language by the ear. Pattern of Intonation contour have been investigated in various Indian languages such as Kannada, Tamil, Gujarati and Hindi[4]. A pattern of a final fall (either a gradual or steep) was identified in sentence types such as neutral, jealousy, hesitation, request and for question, anger + question, frustration, accusation a final rise contour was identified in Kannada[5]. Studies on expression of emotions of anger, frustration, grief, joy, jealousy, neutral, surprise and worry were carried out in Tamil, Malayalam, Telugu and Bengali languages. It was found that, a final fall Fo pattern was

observed in most of the emotions in Tamil. However, the emotion fear was characterised by final rise pattern[6]. Intonation pattern of Malayalam and Telugu languages were characterised by final fall patterns for all types of emotions[7][8]. In Bengali, all emotions had terminal falling Fo patterns except for the emotions fear and surprise[9]. The intonation of various emotions such as anger, happiness, sadness and neutral in Punjabi language revealed raising Fo patterns for emotions with more excitement whereas the less excited emotion was spoken with falling contour.[10] But, these intonation patterns are not strictly universal. For example, exclamatory sentences had a raising pattern in Kannada and Konkani[3], which is a similar finding reported for English,[11] whereas, a falling pattern was seen for exclamatory sentences in Tulu. Similar results were reported in French and German respectively[12][13].

The terminal intonation patterns of different sentence types like declaratives, exclamatory, interrogatives, and imperatives were taken and recorded in three languages Kannada, Tulu and Konkani were examined[14]. F0 patterns showed that declaratives and imperatives had falling contours in all languages. Exclamatory sentences had raising contours in Kannada and Konkani, but falling contour in Tulu. Interrogatives had raising patterns across all languages, except for males in Kannada. The production of sentences in Kannada, Konkani and Tulu indicated differences in the terminal F0 pattern across the different sentence types.

A study done on Japanese and Russian languages reported that there is an increase in the height or magnitude of a rise for the intonation pattern of a declarative sentence in both languages[15]. For the language English there is a raising terminal contour in the exclamatory sentence[16].

A study on perceptual correlates of sentence-type intonation in French indicated that in French language declaratives and exclamatives were of falling intonation pattern, interrogatives were of rising and imperatives split between falling and rising contours depending on their specific functions[17]. Falling intonation is reported to indicate a declarative utterance, while a rising intonation contour declares an interrogative utterance in German[18].

Dialect is a particular form of a language which is peculiar to a specific region or social group. A study on the role of intonation in language and dialect discrimination by adults was examined[19]. In their study they investigated whether listeners are relying on pitch cues for language discrimination. They acoustically analyzed American English and German, and American and Australian English to demonstrate that these pairs are distinguishable using either rhythmic timing or pitch information alone. Then, American English listeners' ability to discriminate prosodically-similar languages was also examined using (1) low-pass filtered, (2) monotone resynthesized speech, containing only rhythmic timing information, and (3) re-synthesized intonation-only speech. Results showed that listeners can use only pitch cues to discriminate between American English and German. Additionally, although listeners are unable to use pitch cues alone to discriminate between American and Australian English, their classification of the two dialects is improved by the addition of pitch cues to rhythmic timing cues. They suggested that, the role of intonation cannot be ignored as a possible cue to language discrimination

The literature review suggests that there are many studies that have been carried out in intonation in various languages. However, limited studies have done to examine the intonation difference with respect to dialects. India is a multilingual country. Most of the Indian languages have different dialects and variations, sometimes very different from each other. Dialects of Kannada fall into four groups[20]. They are Coastal dialects, Northern Dialects, South-eastern Dialects and southern dialect. Prosodic variations have been well documented in many foreign languages across various dialects[21][22]. In Indian context, such studies are limited.

Need for the study - Studying intonation patterns in different dialects will help a speech language pathologist to understand the normal and abnormal aspects of prosody in a specific region or social group. This will further help in the assessment and management of prosodic errors in individuals with various speech and language disorders in a group of people belonging to a specific region. This would also shed

some light on the parameters of prosody that need to be incorporated for the synthesis of speech in the Indian languages. Several studies have been carried out to determine the intonation pattern in Kannada language. However no studies have been compared the intonation pattern between different dialects in Kannada. Hence the present study focused to determine the intonation patterns in Bangalore dialect Kannada and Dharwad dialect Kannada using acoustical methods in four different emotions such as 'happy', 'sad', 'anger' and 'question'.

Aim of the study-To investigate and compare the terminal contour of intonation between Bangalore dialect Kannada and Dharwad dialect Kannada in sentences depicting emotions such as 'happy', 'sad', 'anger' and 'question'.

2. METHODS

Development of the stimulus - Four sentences depicting emotions such as happy, sad, anger and question were chosen for the study and they were |ap·a| |nangɛ| |h□sa| |bat·ɛ| |k□dsɪd□ru|, |nʌn·a| magangɛ| |kɪvɪnɛ| |kɛ:lɪst□ɪl·a|, |nɪn·a| |mukha| |nangɛ| |mat□□ɛ| |t□o:rɪsbɛda|, |ɪl·ɪnd□a| |ɛʃtu| |d□u:ra| |ɪd□ɛ| |ma□isu:ru| respectively. All the sentences were having a mean length of utterance of about 4 to 5 words.

Stimulus recording - Two trained theatre artists were served as subjects for stimulus recording. The subject one was a native speaker of Kannada and from southern part (Bangalore) of Karnataka. The subject two was also native speaker of Kannada and he belonged to northern part (Dharwad) of Karnataka. The stimulus recording was carried out in a sound proof room. Before recording the stimuli both the subjects were seated comfortably and explained regarding the purpose of the study. Sony digital voice recorder was used for recording the stimulus and it was kept at a distance of approximately 5-6 inches away from the subjects mouth. The four sentences chosen for the study were then given to each of the subjects. The subject one was instructed to utter the sentences in the intended emotions thrice in Bangalore dialect Kannada and the subject two was also instructed to utter the sentences thrice in the intended emotions in Dharwad dialect Kannada. Hence a total of twenty four utterances depicting emotions such as 'happy', 'sad', 'anger' and 'question' were recorded out of which 12 sentences were in Bangalore dialect and 12 were in Dharwad dialect.

Perceptual evaluation - These recorded audio samples were given for perceptual evaluation to three experienced Speech- Language Pathologists and were instructed to rate the sample with respect to the intended emotion as good, average and poor. Based on the perceptual analysis rating, the investigator selected the best recording from each emotions in both Bangalore dialect and Dharwad dialect Kannada and these utterances were considered for further analysis .Thus the study included 8 sentences depicting emotions such as 'happy', 'sad', 'anger' and 'question' among which four sentences were uttered in Bangalore dialect Kannada and remaining four in Dharwad dialect Kannada.

Acoustic analysis - PRAAT software was used for the acoustic analysis. The highest and lowest F0 was noted in each sentence to calculate F0 range. The intonation contours were obtained by analysing the terminal syllable F0 contour for each sentence of Bangalore dialect Kannada and Dharwad dialect Kannada. A difference of 20 Hz or more between two levels was considered adequate for considering that as a rise or a fall and only change of less than 20 Hz was considered as steady[23]. For example the pitch curve extracted from praat software for the sentence "|nɪn·a| |mukha| |nangɛ| |mat□□ɛ| |t□o:rɪsbɛda| as uttered by a subject one in south dialect is displayed below.

The PRAAT software enables simultaneous visualization of the fundamental frequency pattern for a given portion of speech signal, the intonation contours and also the waveform. A vertical cursor, which would be moved horizontally, was used to mark specific portion of the waveform, highlight and listen to the signal present in the marked portion of the waveform and by clicking the 'pitch' button the minimum fundamental Frequency (in Hertz), the maximum fundamental Frequency (in Hertz) and the average
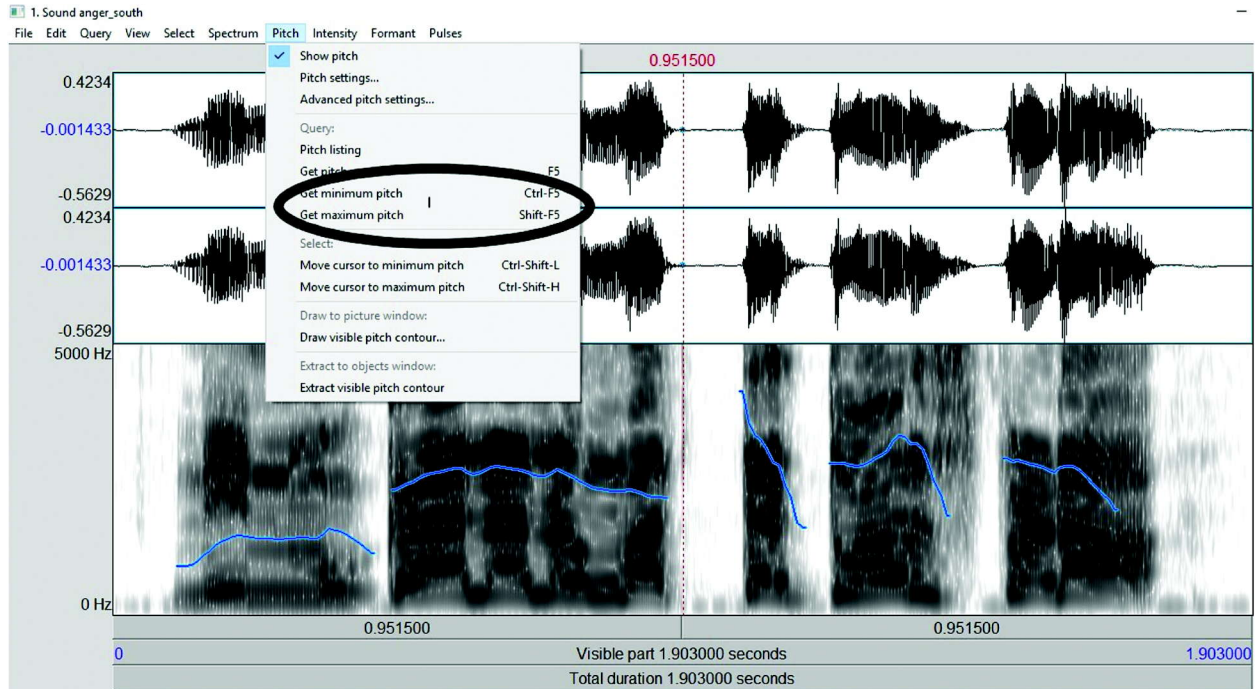
fundamental frequency (in Hertz) between these points could be noted as depicted in above figure. For each sentence, the range of frequency variations was calculated by subtracting the lowest frequency from the highest frequency. Thus the intonation contours obtained for all the sentences were compared to find out the intonation of utterances in each emotion of Bangalore dialect Kannada and Dharwad dialect Kannada.

3. RESULTS AND DISCUSSIONS

Acoustic analysis revealed differences in the intonation contours between Bangalore dialect and Dharwad dialect Kannada. Table 1 and Graph 1shows the F0 range of Bangalore dialect and Dharwad dialect Kannada.

Table 1. The F0 range of the emotions

Emotions	F0 Range	
	Dharwad dialect	Bangalore dialect
Anger	114 Hz	273 Hz
Happy	167 Hz	254 Hz
Question	121 Hz	126 Hz
Sad	92 Hz	100 Hz

Fo range was found to be higher for all the emotions in Bangalore dialect Kannada. This indicates more pitch variations in Bangalore dialect Kannada when compared to Dharwad dialect. The f0 range was found to be highest in emotion Anger in south dialect, whereas more difference in f0 range was found in the emotion Happy in Dharwad dialect Kannada. The lowest range of f0 was found in the emotion sad for both Bangalore and Dharwad dialect Kannada.

The results also indicated differences in intonation contours between Bangalore Dialect and Dharwad dialect Kannada in all the emotions. Table 2 shows the most common pattern and the terminal syllable intonation pattern for all the emotions considered in the present study in both the dialects.

Table 2. Most common pattern and the terminal syllable intonation pattern

Emotions	Most common pattern		Terminal syllable pattern	
	Dharwad dialect	Bangalore dialect	Dharwad dialect	Bangalore dialect
Anger	Fall	Fall	Flat	Fall
Happy	Rise-Fall	Fall	Rise-Fall	Rise
Question	Fall	Rise	Flat	Rise
Sad	Rise-Fall	Flat	Flat	Flat
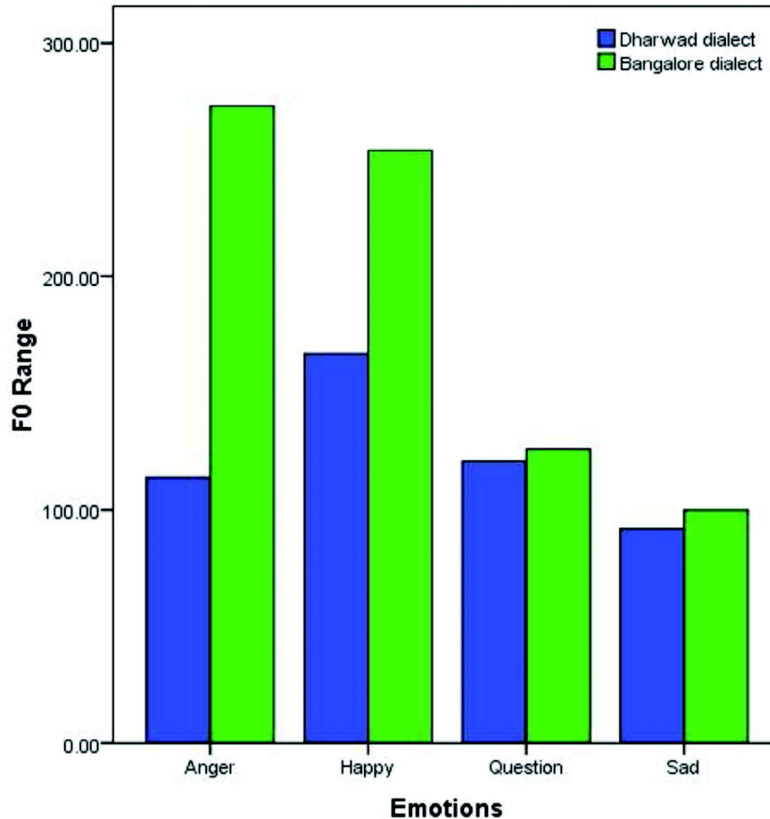
Graph 1: The F0 range of the emotions

For emotion Anger the most common contour was found to be falling in both Bangalore and Dharwad dialect Kannada, however the terminal syllable contour of final word in anger was found to be flat in Dharwad dialect and fall in Bangalore dialect Kannada. For the emotions happy and sad compound tone (rise, fall) was found in Dharwad dialect Kannada. Whereas the Bangalore dialect Kannada showed the most common intonation contours of fall and flat for the emotions happy and sad respectively. A falling pattern was found in the emotion 'question' in Dharwad dialect Kannada and a rising pattern was found in Bangalore dialect Kannada.

The results yielded many points of interest. Firstly, the results of acoustic analysis indicated the presence of compound tones to be more in Dharwad dialect when compared to Bangalore dialect Kannada. Second, there were variations observed in the terminal syllable of each utterance between the dialects in all emotions except for sad, where it was found to be flat in both the dialects. Finally, the range of pitch variation over the utterances was found to be more in Bangalore dialect than Dharwad dialect Kannada.

4. CONCLUSION

The present study attempted to investigate and compare the intonation contours in four types of emotions such as 'happy', 'sad', 'anger' and 'question' between Bangalore dialect and Dharwad dialect Kannada using acoustical methods. The results indicated differences in the intonation pattern between the dialects. The results also indicated presence of compound tone more in Dharwad dialect Kannada compared to Bangalore dialect Kannada. However the results can be generalized only with larger samples.

Studying the aspects of intonation patterns in different dialects provide an understanding of normal and abnormal aspects of prosody in a specific region or social group to a Speech Language Pathologist. It is essential to know the normal prosodic aspects for assessment and management of individuals with prosodic impairment. This also provides information for synthesising speech for various research purposes.

5. REFERENCES

[1]   W. A. Anisworth, 1976. *Perception of prosodic features*. Terhaar (Ed), London: Pergamon Press

[2]   L. Pisoni and Saweesh, 1975. Intonation in Kannada. In Manjula, R. *Unpublished Master's Dissertation*, University of Mysore.

[3]   M. M. Mathew and J. S. Bhat, 2010. Nature of Sentence Intonation in Kannada, Tulu and Konkani. *Language in India,* **10**, 15-25.

[4]   N. P. Nataraja, 1981. Intonation in four Indian languages under five emotional conditions. *Journal of AIISH,* **12**, 22- 27.

[5]   H. N. Nandini, 1985. Some prosodic aspects in Kannada. *Research at A.I.I.S.H*: Dissertation Abstracts, 82, Vol II. (D 134).

[6]   M. J. Varshini and N. P. Nataraja, 2000. Some aspects of intonation in Tamil. *Dissertation submitted to University of Mysore,* Mysore.

[7]   N. Mini and N. P. Nataraja, 2000. Intonation in Malayalam- Some aspects. Research at A.I.I.S.H, *Dissertation Abstracts,* **IV**, 90-91 (D 402).

[8]   C. S. Sandhya and N. P. Nataraja, 2000. Intonation in Telugu- Some aspects. Research at A.I.I.S.H, *Dissertation Abstracts,* **IV**, 90-91 (D 401).

[9]   S. Saha and N. P. Nataraja, 1999. Intonation in Bengali- some aspects. Research at A.I.I.S.H, *Dissertation Abstracts,* **IV**, 82 (D 396).

[10]   H. Dawood, R. Shahid and R. Touqeer, 2004. *From Annual Report*: Intonation Patterns in Punjabi. from http://www. crulp.org/research/reports/streport/

[11]   D. Bolinger, 1972. *Intonation: Selected readings. England*: Penguin Books Ltd.

[12]   D. Bassano and M. I. Mendes, 1994. Perceptual correlates of sentence-type intonation in French. *Journal of Phonetics,* **44**, 132-144.

[13]   V. Raithel and M. F. Hielscher, 2004. Emotional and linguistic perception of prosody. *Folia Phonatrica logop*, **56**, 7-13.

[14]   Mili Mary Mathew and Jayashree S. Bhat, 2010. Nature of Sentence Intonation in Kannada, Tulu and Konkani. *Language in India,* **10**(11), 15-25.

[15]   V. Markowa, 2000. Perceptual correlates of sentence type intonation in Russian & Japanese. *Journal of phonetics,* **29**(2), 137-154.

[16]   D. Bollinger, 1972. Intonation: selected readings. England: Penguine Books Ltd.

[17]   D. Bassano and M. I. Mendes, 1994. Perceptual correlates of sentence-type intonation in French. *Journal of phonetics,* **44**, 132-144.

[18]   V. Raithel and M. F. Hielscher, 2004. Emotional and linguistic perception of prosody. *Folia Phonatrica logop,* **56**, 7-13.

[19]   Chad Vicenik and Megha Sundara, 2013. The role of intonation in language and dialect discrimination by adults. *Journnal of phonetics,* **41**(5), 297-306.

[20]   Michail Andronov, 2003. A comparative grammar of the Dravidian languages. Harrasowitz Verlag. Wiesbaden.

[21]   J. I. Hualde, G. Elordieta, I. Gaminde and R. Smiljanic, 2002. From pitch-accent to stress-accent in Basque and the typology of accentual systems. In: Gussenhoven C, Warner N, editors. *Papers in Laboratory Phonology*. Cambridge University Press; Cambridge. **7**, 547-584.

[22]   J. Bishop and J. Fletcher, 2005. Intonation in six dialects of Bininj Gun-wok. In: Jun S-A, editor. *Prosodic Typology*. Oxford University Press; New York. pp. 331-361.

[23]   Rajesh, 1998. Analysis of prosodic aspects aspects of Kannada - In hearing impaired children. *Unpublished Master's Dissertation*, University of Myosre.

Development of multi-channel data logger
for passive acoustic measurements

William A. Fernandes*, Yogesh Agarvadekar and Bishwajit Chakraborty
CSIR-National Institute of Oceanography
Dona Paula, Goa. 403004
william@nio.org

ABSTRACT

Recording of passive acoustic data involves a listening device along with an instrumentation system. The passive listening device transforms mechanical disturbances to electrical signals. The subsequent sampling and logging of the transformed data is accomplished by employing the instrumentation system. One such system is the Low cost "Multi-Channel Data Logger" (MCDL) that is indigenously developed at CSIR-National Institute of Oceanography with a capability to record 8- channels of passive acoustic signals simultaneously. Here we have presented the designed and developed MCDL system interfaced with a six channel hydrophone array to log ambient noise data from the underwater environment and also connected with dual low cost high sensitivity microphones for recording terrestrial ambient noise signals. The laboratory tests & field trials along with the data analysis results are presented to demonstrate the MCDL's multi-platform functionality.

1. INTRODUCTION

In marine environment the sound signals are generated by various sources (surface as well as undersea) and are collectively called as marine ambient noise (AN). AN is sometimes classified as geo-phonic, bio-phonic and anthro-phonic. These underwater ambient noise signals may travel longer distances and therefore can be studied for number of applications such as underwater object detection, tracking of marine habitats and identification etc. Moreover, the terrestrial applications include forest soundscape studies using animal/ bird sounds, for species identification, quantification studies and protection. The birds migrate due to the effects of climate change, reaching at their breeding grounds sooner as global temperature rise[1]. Hence birds migration pattern does provide the signatures of climate change. However, long term monitoring of environmental parameters may be used for climate research[2]. The Study of traffic and pollution data can be used to comprehend the environmental parameters. All the above mentioned research studies can be undertaken by implementing economically low cost data loggers within the region of interest.

In this work, we present the low cost Multi-channel Data Logger (MCDL) system and the passive acoustic data acquired from laboratory tests to field trials held within the Goan boundaries, along with a demonstration data recorded at Radhanagri wildlife sanctuary, Maharashtra. It may be stated here that the developed low cost instrumentation system can be employed at different locations for monitoring species (marine as well as terrestrial) and also the marine traffic by utilizing multi-channel facility of the MCDL.

2. MATERIALS

The self contained battery operated autonomous Multi-Channel Data Logger (MCDL) designed around Teensy 3.6 cortex-M4F ARM (Advanced RISC Machine) processor board (www.pjrc.com). The Teensyduino software provides integrated support for Teensy microcontrollers within Arduino IDE software platform by adding microcontroller specific libraries and the compiled program download utility that loads the program to the microcontroller memory. The C program compiled either on Linux using GNU gcc compiler or Windows is utilized to convert the recorded binary formatted data to ASCII file format. The microcontroller is interfaced with 8- channel Successive Approximation Register (SAR) - Analog to Digital Converter (ADC) using byte transfer mode that transfers data from ADC to microcontroller. At the time of acquisition every sample ensemble of 8- channels, 16 bytes are transferred from ADC to microcontroller. In this mode a sampling rate of 100 kHz was obtained. The MCDL block diagram demonstrates the total system functioning protocol (fig.1). The system is powered through 8D cells each of 1.5V alkaline batteries having total capacity of 7.2AH, may provide approximately 40 hours of continuous sampling of 8 channels at a maximum sampling rate of 100 kHz. In active mode, it consumes maximum of 150 mA, while the sleep mode consumption is less than 0.5 mA approximately.
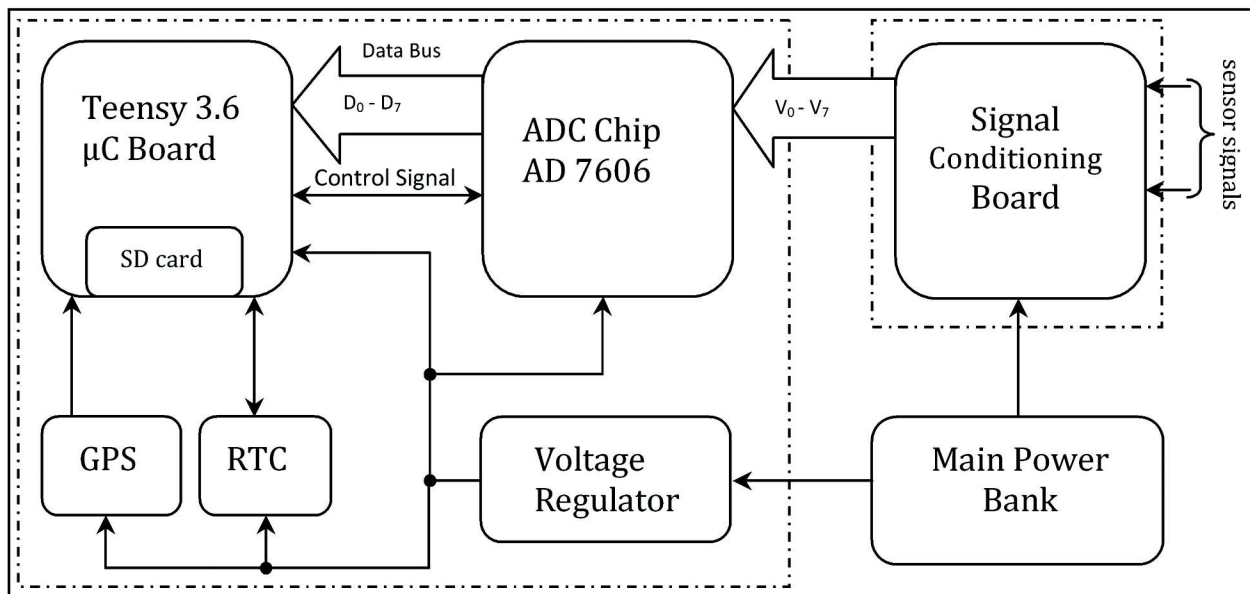
Fig. 1. Showing MCDL functional block diagram

For field trials and the demonstration, the sample rate of 25kHz was preferred for recording of bio-phonic and anthropogenic process generated acoustic signals. The marine AN data was acquired using single wideband C55 hydrophone (www.cetaceanresearch.com) for sampling duration of 30 seconds in every 1 minute. However, the laboratory test data was acquired for duration of 10 seconds in every 1 minute. The terrestrial ambient noise was also recorded by interfacing locally available low cost high sensitivity condenser microphones with the above mentioned configuration. The system is designed for short term deployments, however long term monitoring is also possible by upgrading the main power bank and its casing. The signal conditioning card consists of eight dual op-amps pairs configured in DC servo amplifier mode to enhance the electrical signal and to reduce the possibility of noise contamination from ancillary environmental factors. The precision Real-Time Clock (RTC) is provided to monitor sampling and recording time intervals together with time stamping the data. The precision RTC is synced with GPS time in every 24 hrs. During acquisition, the incoming signals are sampled, digitized and stored in the storage media of size 64 GB (upgradable up to 128 GB). The system features flexible and user customizable

configuration with sample rates as high as 100 kHz with a file size of 96 MB for 60 seconds. The main 16-bit logger board along with GPS, signal conditioning and main power bank are packed in water proof enclosure. The water-proof interface is also provided on the enclosure. The system is fully water-tight and therefore can be installed on any fixed/floating platform for the acquisition of AN data.

3. METHODS

After successful initial tests of the MCDL system that were carried out by interfacing sine signals to each channel, the laboratory tests were performed, interfaced with single wideband C55 hydrophone deployed in water contained glass aquarium of dimension 50 cm × 25 cm × 25 cm approximately. The aerator was installed and adjusted to generate air-bubbles in water medium, producing signals that are transformed and stored within the logger memory. During second phase of testing at the pool site, the Vertical Linear Array (VLA) of 6-channel hydrophones together with dual microphones were connected to MCDL for a short period of time, so as to check system's versatility. However, during tests and trials, the data was acquired leaving unused channels opened. The field trial at Dona Paula jetty was executed by interfacing single wideband C55 hydrophone (leaving unused channels opened), deployed at 2.5 m below the water surface and configured to record 30 seconds of sampled data at 25kHz for every 1 minute. However due to shallower depths and higher currents at Cortalim jetty, the hydrophone depth was limited to 1.5 m approximately.

Subsequently, the system demonstration was also arranged in the month of March, 2017 at Radhanagri wildlife sanctuary to study forest soundscape by capturing terrestrial ambient noise (birds, animals and wind generated sounds) data employing low cost higher sensitivity microphones. At dusk, the MCDL was placed at the irrigation department guest house with in the sanctuary with the intention to record early morning bird sounds, but the cricket chorus sound was evident during the period. However, at dawn many birds sound signals were observed. The marine AN data was also logged (as a part of the demonstration) by interfacing single wideband C55 hydrophone, placed approximately at 1 meter below the water surface in the Radhanagri dam for a short span of time. The analyses of the logged data were performed by utilizing Matlab (www.mathworks.com) computational platform employing basic signal processing tools.

4. RESULTS AND DISCUSSIONS

The design of 16-bit MCDL composed of integrated sensor (channel) interface, ADC & signal conditioning circuit board along with Teensy 3.6 cortex-M4F ARM micro-controller and storage. The system utilizes 8- channel SAR - ADC that employs byte transfer mode for data transfer from ADC to microcontroller. At the time of acquisition every sample ensemble of 8- channels, 16 bytes are transferred from ADC to microcontroller. In this mode a sampling rate of 100 kHz was obtained. The system has better features particularly towards sample rates, data storage capabilities and improved signal conditioning per channel. The configuration (config.txt) file is simple text format file that holds the settings (File prefix; sampling interval; sample rate; recording interval) and can be easily altered by the user using available text editors. However in the present data, the configuration file was set as per the requirement and unaltered for most of the tests except for file prefix & sampling interval. The MCDL is powered through 8 D cells each of 1.5V alkaline batteries having total capacity of 7.2 AH. In active mode, it consumes maximum of 150 mA, while the sleep mode consumption is less than 0.5 mA approximately. The system presently provides 64 GB microSD card (data storage media) that may be upgradable upto 128GB. Moreover it features flexible and user customizable configuration with sample rates as high as 100 kHz with a file size of 96 MB for 60 seconds.

The analyses of the data recorded in laboratory condition have shown the train of bubble blast sound signals Fig. 2(a). The spectrogram i.e., Short Time Fourier transform (STFT) of the laboratory recorded time series acoustic data acquired using the Multi-Channel Data Logger is presented in Fig. 2(b) in
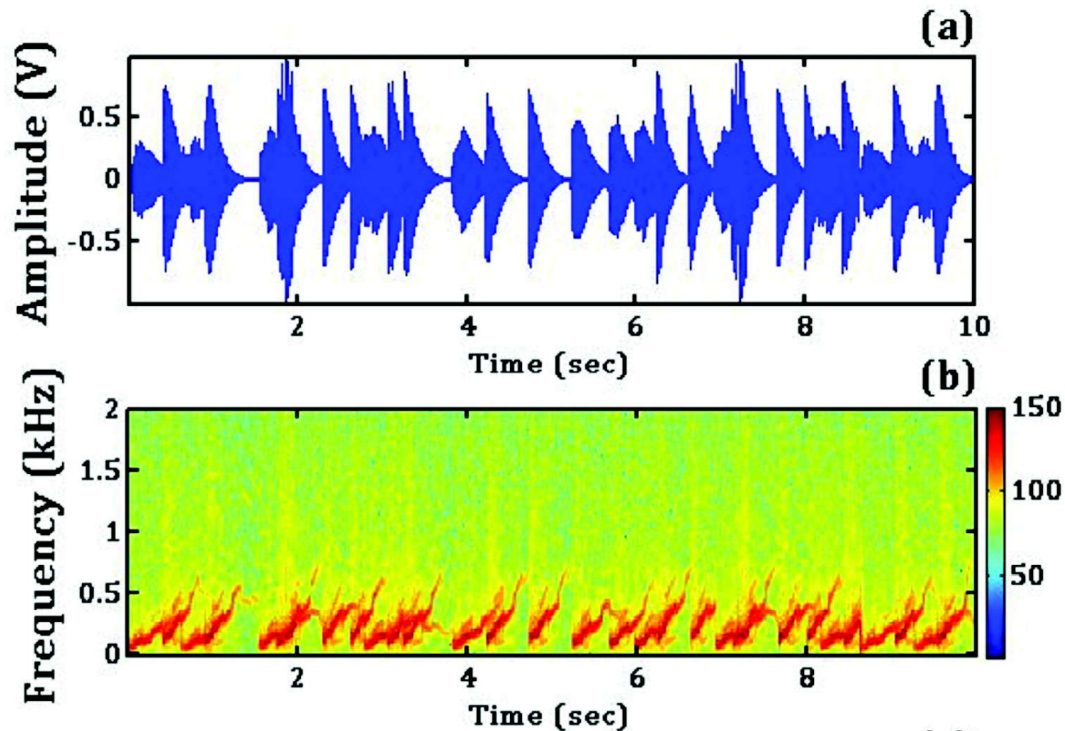
Fig. 2. Showing (a) Time series and (b) frequency spectrum of the bubble
blast sounds recorded in laboratory

terms of frequency (Hz) versus time (sec). Higher signal strengths of 132.7 dB are observed at 147 Hz. It was also observed that varying the bubble size produces variation in the signal strengths and also to its peak frequency[3]. In the second phase of testing, the MCDL was operated with an VLA of 6-hydrophones and dual microphones as an experiment to record underwater as well as land based AN signals. The logged array data have not shown much variations, however the microphones have recorded human talks and bird chorus.

The AN data acquired during field trials at Dona Paula jetty has shown jet skis underwater broadband sound signal, overlain with harmonically related tonals (ranging from 300 Hz to 5kHz that can be seen from Fig. 3(b)[4] and also the snapping shrimp noise, which is a dominant source of mid- frequency ambient noise[5]. The trial data recorded at Cortalim floating jetty has provided indication of piling information which was from the piling station positioned diagonally (~500 m) across the Zuari river banks, having signal strengths of 133 dB at the lower frequency of 48.83 Hz, observed through spectrogram (STFT) and Welch's power spectral density estimate (Fig. 4)[6]. Furthermore the demonstration data acquired at Radhanagri wildlife sanctuary, has shown significant improvement in capturing birds sound signals despite of rough windy conditions[7]. Moreover, the logged data have revealed the low amplitude signatures from birds which were otherwise ignored due to heavy noise induction. As it was equipment demonstration, other parameters were not necessary and hence the spot weather data was not collected. The terrestrial ambient noise data recorded at other locations within the Sanctuary, provided better results due to stable weather conditions or may be for the reason that the system installation was at lower elevation (Fig.5). However the source identification is not the purpose of this study. The recorded ambient noise during the transition period from dusk to night, the cricket noise signal was observed [8 & 9]. The cricket generates the sound pulse by the effect of scissoring movements of the two wings having a series of harmonically related frequency components that were noticed at 3.5 kHz, 6.7 kHz and 10.4 kHz (fig. 6)[8]. However the peak of the spectrum was found to be at 6.7 kHz.
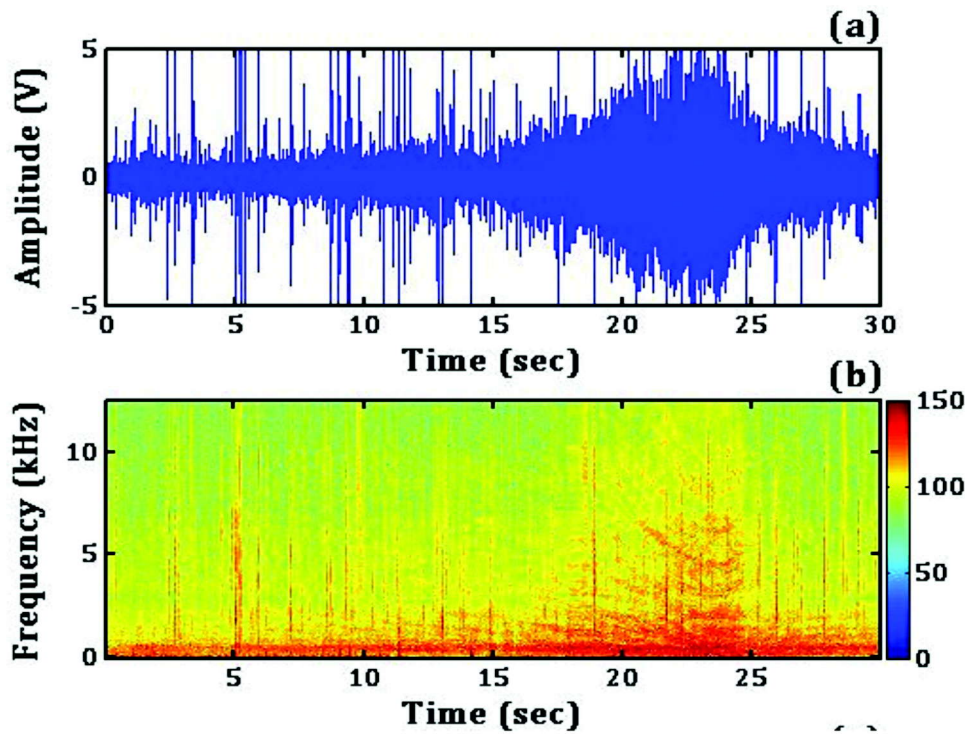
Fig. 3. Showing (a) Time series and (b) frequency spectrum of the Jet skis recorded at Dona Paula jetty
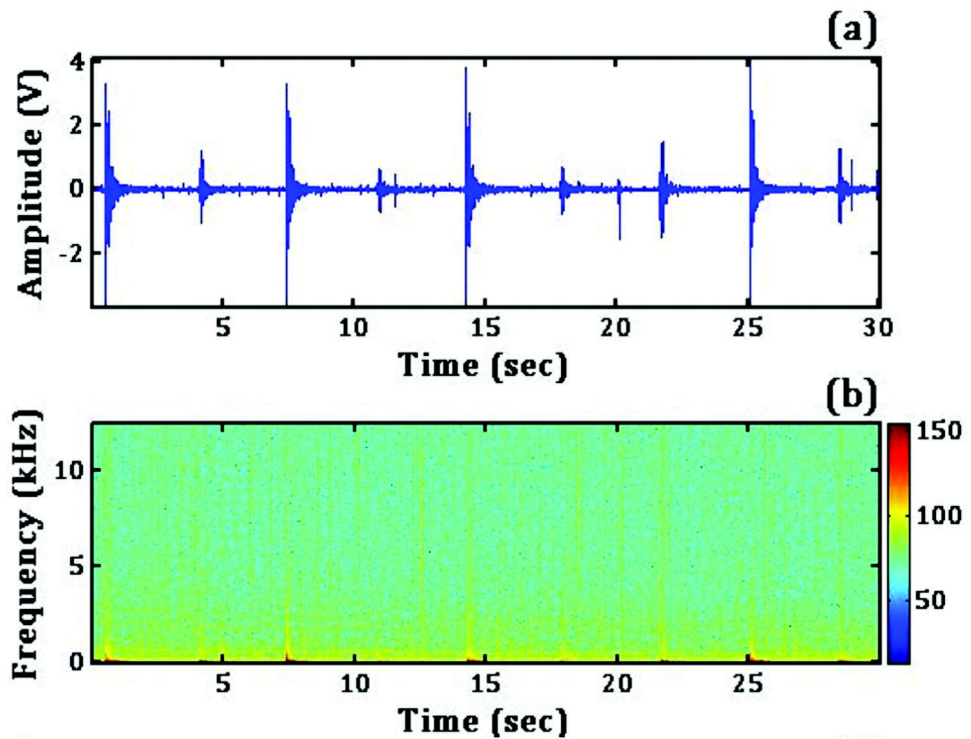
Fig. 4. Showing (a) Time series (b) frequency spectrum of the pile driving
noise signals recorded at Cortalim private jetty

William A. Fernandes, Yogesh Agarvadekar and Bishwajit Chakraborty
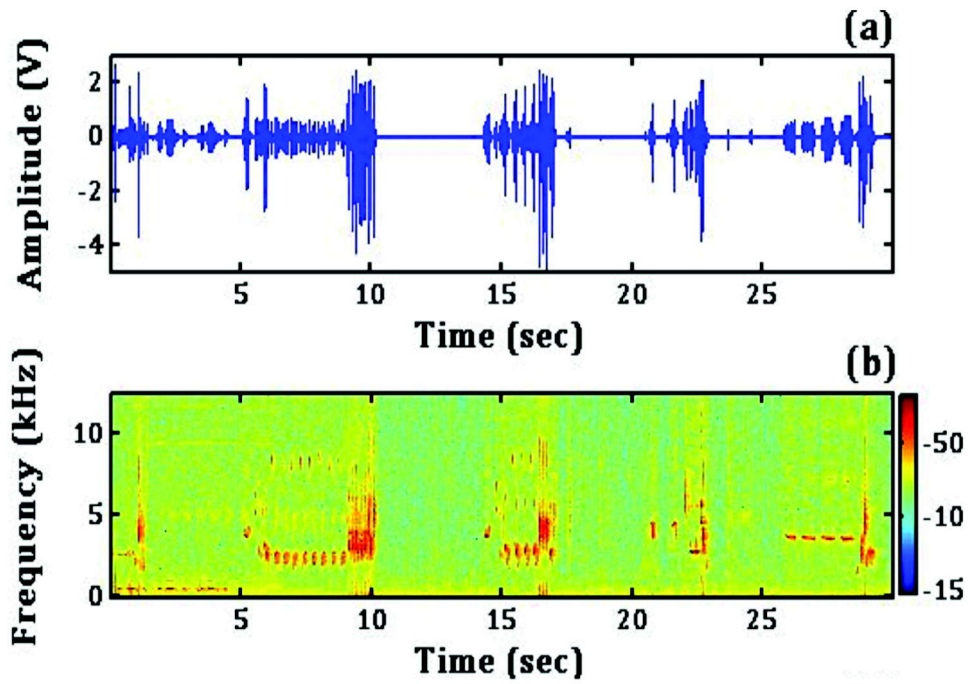
Fig. 5. Showing Time series & Frequency Spectrum of the small farm birds sound signal acquired at Irrigation department guest house, Radhanagri
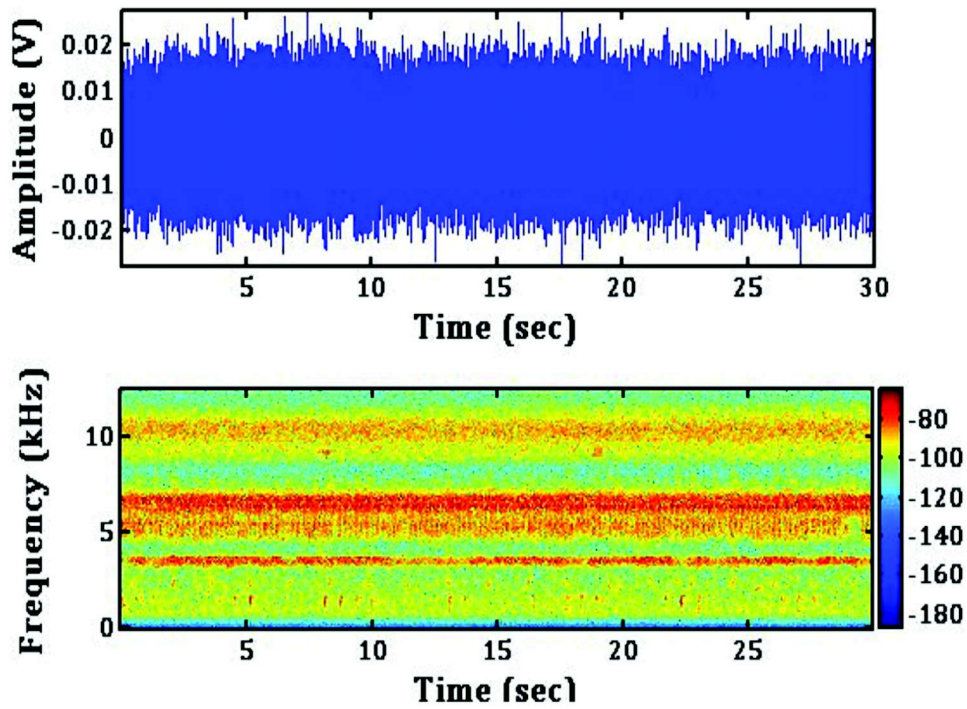
Fig. 6. Showing Time series & Frequency Spectrum of the cricket sound signal acquired at Irrigation department guest house, Radhanagri

5. CONCLUSION

In this study , we presented indigenously developed Multichannel Data Logger (MCDL) that was employed to acquire AN data at various locations. The results were demonstrated through specified figures. The VLA of 6-channel hydrophones together with dual microphones were connected to check MCDL's flexibility in recording underwater as well as land based AN signals, however logging of weather data was not attempted. The SAR-ADC & signal conditioning board has provided better results as can be seen from the figures (oscillograms and spectrograms). The AN data acquired during system demonstration at Radhanagri wildlife sanctuary have shown the evidence of small farm birds. Additionally, the cricket noise sounds were also observed. Finally, the results have illustrated that the system is capable of recording quality data under the effects of moderate weather conditions.

6. ACKNOWLEDGMENT

7. REFERENCES

[1]   E. Lehikoinen, T. H. Sparks, A. P. Møller, W. Fiedler and P. Berthold, 2010. "Changes in migration, Birds and limate change", *Oxford: Oxford University Press,* pp 89-112.

[2]   N. Rubolini, N. Saino and A.P. Møller, 2010. "Does migratory behaviour constrain the phenological response of birds to climate change?", *Clim Res*, **42**, 45-55.

[3]   S. Husin, A. Addali and D. Mba, 2011. "Acoustic frequency for bubble size correlation using acoustic emission", *Sixth International Conference on Computational and Experimental Methods in Multiphase and Complex Flow*, At Kos, Greece.

[4]   Christine Erbe, 2013. "Underwater noise of small personal watercraft (jet skis)" *J. Acoust. Soc. Am.* **133**, EL326.

[5]   John A. Hildebrand, 2009. "Anthropogenic and natural sources of ambient noise in the ocean" *Marine Ecology Progress Series,* **395**, 5-20.

[6]   Donatas Bagočius, 2015. "Piling underwater noise impact on migrating salmon fish during Lithuanian LNG terminal construction (Curonian Lagoon, Eastern Baltic Sea Coast)", *Marine Pollution Bulletin*, **92**, 45-51.

[7]   C. M. Harris, 1966."Absorption of sound in air versus humidity and temperature", *J Acoust Soc Am,* 40, 148-159.

[8]   Gerald Pollack, 2014. "Cricket acoustic communication", *Scholarpedia*, **9**(2), 11999.

[9]   J.-F. Augoyard, 1998. "The cricket effect. Which tools for the research on sonic urban ambiences?", "*Stockholm, Hey Listen*!" Conference, Royal Swedish Academy of Music.

Studies of ultrasonic and acoustic parameters of copper (II) surfactant of mustard and groundnut oils treated at different temperatures

Renu Bhutra[1], Rashmi Sharma[2] and Arun Kumar Sharma[3],*

Department of Chemistry
[1]Rajesh Pilot Govt. Polytechnic College, Dausa-303303, Raj., India
[2]S.P.C. Govt. College, Ajmer-305001, Raj., India
[3]Govt. P.G. College Jhalawar-326001- Raj India
sharmaarun423@gmail.com

ABSTRACT

Colloid chemical behavior and micellar characteristics of Cu (II) soaps derived from mustard and groundnut oils, (fresh oils and treated with 15 and 60 min.) at high temperature in benzene have been investigated and verified by ultrasonic velocity measurement. From these values, various acoustic parametershave been calculated. The results have been analyzed byMasson equation. The results have been explained on the basis of solute-solvent interactions. The decrease in β and L_f with increasing concentration of the complex is indicating that there is sufficient solute- solvent interaction due to which micellar alignment is considerably affected.

1. INTRODUCTION

Now a day ultrasonic is considered to be a powerful tool in research activity in various fields. Ultrasonic investigations have established its versatility to furnish information as to the understanding of solute-solvent interaction. A number of workers[1-5] have discussed the physico-chemical aspects of ultrasonic velocity and related parameters. The Gruneisen parameter and internal pressure obtained from ultrasonic velocity and density data play a significant role in understanding internal structure, clustering phenomenon and quasi-crystalline nature of binary mixture[6-10]. Ultrasonic measurements have also been used to determine solvation number in aqueous media[11-13]. Ultrasonic investigation of liquid mixture have significant importance in understanding intermolecular interaction between the component molecules as that finds application in several industrial and technological processes[14-15]. Derived parameters from ultrasonic velocity measurements provide qualitative information regarding the nature and strength of molecular interactions in liquid mixtures[16-17]. The present work deals with the determination of ultrasonic velocity measurements which have been used to obtain information regarding various acoustic parameters and solute-solute interactions of copper (II) surfactants of mustard and groundnut oils (fresh oils and treated with 15 and 60 min.) at high temperature in non-aqueous solvent benzene at 303.15 K to access the effect of solvent molecules on the micellar nature of solute molecule[18-19]. The studies have also been done to understand the nature of the solution and observed that the increase in the internal pressure and in lowering the compressibility of the solution. The studies were done in non-aqueous solvents (benzene) to access the

effect of the micellar nature of solute molecule and solute-solute interactions. Because the synthesized compound is maximum soluble in benzene. This information is of fundamental importance for understanding solute-solute, solute-solvent interactions in solutions below and above critical micelle concentration and the structural aspects of the micelle. It is anticipated that it will generate a new hopes in various industrial and analytical applications of the newly synthesized surface active agrochemicals.

2. EXPERIMENTAL

All the chemicals used were of LR/AR grade. Copper soap was prepared by earlier reported methods [20]. All the soaps are stable at room temperature, their physical parameters and composition of oils are discussed in Table -1-2. The Cu (II) soaps are abbreviated as follows:

1. Copper - Mustard soap (CM)
2. Copper - Groundnut soap (CG)
3. Copper - Mustard soap treated for 15 min at high temperature. (CM_{15})
4. Copper - Groundnut soap treated for 15 min at high temperature. (CG_{15})
5. Copper - Mustard soap treated for 60 min at high temperature. (CM_{60})
6. Copper - Groundnut soap treated for 60 min at high temperature. (CG_{60})

Ultrasonic interferometer from Mittal Enterprises, Model M-82 with accuracy of $\pm$ 0.03% was used for the measurements of ultrasonic velocities in various solutions at a fixed frequency 2MHz. Water maintained at 303.15 K temperature in a thermostat was passed through the jacket of the cell before the measurement was actually made. The total distance d (1 cm) and wavelength λ are co related by following relation:

$$\lambda = 2d/n \tag{1}$$

The ultrasonic velocity U in the solution can be calculated by following relation:

$$U = \lambda \times f \tag{2}$$

3. RESULTS AND DISCUSSIONS

3.1. Acoustic parameters

Ultrasonic investigations have important parameter to understanding of solute - solvent interactions. A

Table 1. Fatty acid composition of oils used for Copper Soap synthesis

Name of oil	% Fatty Acids					
	16:0	18:0	18:1	18:2	18:3	Other Acids
Groundnut Oil	10	4	61	18	-	C_{20}-C_{24} 7%
Mustard Oil	2	1	25	18	10	C_{20}-C_{22} 41%

Table 2. Analytical and physical Data of Copper Soaps derived from treated and untreated oils

Name of Copper Soap	Color	Melting point (in °C)	Yield %	Metal %		S.V.	S.E.	Average Mol. Wt.
				Found	Calculated			
CG	Green	98	70	10.15	9.724	188.70	297.29	656.08
CM	Green	92	72	9.58	9.110	175.80	319.10	699.72
CG_{15}	Green	105	75	11.90	11.936	238.40	235.31	532.12
CM_{15}	Green	84	74	12.48	12.549	266.47	210.53	482.56
CG_{60}	Green	68	76	13.59	13.744	280.00	200.35	462.20
CM_{60}	Green	61	78	12.96	13.138	260.00	215.76	493.03

number of workers have discussed the physicochemical aspects of ultrasonic velocity and related parameters. It has been used to determine the solvation number[21].

The specific acoustic impedance Z, adiabatic compressibility β, intermolecular free length L_f, apparent molar compressibility ϕ_k, molar sound velocity R and primary solvation number S_n have been calculated by using the following relationships[22].

$$Z = U\rho \tag{3}$$

$$\beta = \frac{1}{U^2\rho} \tag{4}$$

$$L_f = K\sqrt{\beta} \tag{5}$$

$$\phi k = \left[1000.\frac{\beta\rho_0 - \beta_0\rho}{c\rho_0}\right] + \frac{\beta M}{\rho_0} \tag{6}$$

$$R = M.(U)\rho_0 \tag{7}$$

$$M = X_1M_1 + X_2M_2 \tag{8}$$

$$Sn = \left[\frac{n^0}{n}\right].\left[1 - \frac{V\beta}{n^0 V^0 \beta^0}\right] \tag{9}$$

Where β_0, β, d_0, d, n_0, n, $\overline{V}_0$ and $\overline{V}$ are adiabatic compressibility, density, number of moles and molar volume of solvent and solute solution respectively. The molar volume of the solvent $\overline{V}_0$ and soap solution $\overline{V}$ may be written as:

$$\overline{V} = X_1M_1 + X_2M_2 / \rho \tag{10}$$

$$\overline{V}_0 = X_1M_1 + X_2M_2 / \rho_0 \tag{11}$$

In equations (10) and (11) M equal to the molecular weight of component and X the mole fraction of the component and subscript 1 and 2 represents to solute and solvent respectively.

The experimental values of u and other parameters for Cu (II) soaps of untreated oils, treated oils for 15 minutes and treated oils for 60 minutesare recorded in Table-(3-8). The data clearly indicate that the values of u, Z, ϕ_k, S_n and R increase whereas the values of β and L_f decrease consistently with increase in the soap concentration. The increase in ultrasonic velocity may be attributed to the solute-solvent interaction. The increase in the values of specific acoustic impedance Z with soap concentration c due to lyophobic interaction between soap and solvent molecules, which increases the intermolecular distance between the molecules and main cause of propagation of ultrasound waves [23].

Table 3. Ultrasonic velocity and other acoustic parameter of copper soap derived from untreated Groundnut oil. (CG)

c (mol l⁻¹)	ρ (g dm⁻³)	u (m s⁻¹)	Z ×10⁻⁵ (g cm⁻² s⁻¹)	β_ad × 10¹¹ (cm² dyne⁻¹)	L_f (A°)	−φ_k × 10⁸	R × 10⁻²	S_n × 10⁻³
0.0015	0.8693	1278.0	1.1109	7.0437	0.5296	58.861	45.241	-18.512
0.0031	0.8696	1282.1	1.1148	6.9966	0.5278	42.853	45.322	-9.178
0.0038	0.8697	1284.1	1.1168	6.9730	0.5269	39.656	45.361	-7.312
0.0077	0.8699	1288.2	1.1207	6.9264	0.5252	23.490	45.512	-3.633
0.0115	0.8694	1294.5	1.1255	6.8637	0.5228	18.969	45.727	-2.401
0.0153	0.8696	1298.7	1.1293	6.8182	0.5210	15.928	45.884	-1.790
0.0230	0.8700	1302.9	1.1335	6.7712	0.5192	11.012	46.144	-1.189
0.0306	0.8706	1307.2	1.1380	6.7222	0.5174	8.684	46.390	-0.888
0.0383	0.8709	1311.5	1.1421	6.6763	0.5156	7.132	46.655	-0.708
0.0459	0.8714	1315.8	1.1466	6.6283	0.5137	6.193	46.905	-0.588

Table 4. Ultrasonic velocity and other acoustic parameter of copper soap derived from untreated Mustard oil. (CM)

c (mol l^{-1})	ρ (g dm^{-3})	u (m s^{-1})	Z $\times 10^{-5}$ (g cm^{-2} s^{-1})	$\beta_{ad} \times 10^{11}$ (cm^2 dyne^{-1})	L_f (A°)	$-\phi_k \times 10^8$	R $\times 10^{-2}$	$S_n \times 10^{-3}$
0.0014	0.8691	1282.1	1.1142	7.0006	0.5280	91.90	45.302	-19.598
0.0029	0.8693	1292.4	1.1235	6.8871	0.5237	83.068	45.459	-9.588
0.0036	0.8695	1294.5	1.1255	6.8635	0.5228	72.216	45.497	-7.637
0.0072	0.8697	1298.7	1.1295	6.8172	0.5210	40.045	45.649	-3.794
0.0108	0.8699	1305.1	1.1353	6.7492	0.5184	31.271	45.828	-2.502
0.0144	0.8704	1307.2	1.1378	6.7236	0.5174	24.060	45.944	-1.872
0.0215	0.8710	1311.5	1.1422	6.6755	0.5156	16.580	46.197	-1.243
0.0287	0.8715	1315.8	1.1468	6.6273	0.5137	12.854	46.448	-0.928
0.0359	0.8722	1320.1	1.1515	6.5785	0.5118	10.661	46.693	-0.739
0.0430	0.8730	1324.5	1.1563	6.5297	0.5099	9.201	46.937	-0.613

Table 5. Ultrasonic velocity and other acoustic parameter of copper soap derived from treated Groundnut oil for 15 Minute (CG$_{15}$)

c (mol l^{-1})	ρ (g dm^{-3})	u (m s^{-1})	Z $\times 10^{-5}$ (g cm^{-2} s^{-1})	$\beta_{ad} \times 10^{11}$ (cm^2 dyne^{-1})	L_f (A°)	$-\phi_k \times 10^8$	R $\times 10^{-2}$	$S_n \times 10^{-3}$
0.0019	0.8691	1273.9	1.1071	7.0904	0.5313	22.23	45.202	-15.225
0.0038	0.8696	1278.0	1.1112	7.0416	0.5295	22.88	45.271	-7.545
0.0047	0.8699	1280.0	1.1135	7.0163	0.5285	23.42	45.299	-6.006
0.0094	0.8700	1286.2	1.1190	6.9481	0.5260	16.90	45.476	-2.972
0.0141	0.8702	1290.3	1.1228	6.9023	0.5242	13.15	45.628	-1.969
0.0188	0.8707	1294.5	1.1271	6.8541	0.5224	11.53	45.764	-1.466
0.0282	0.8716	1298.7	1.1319	6.8028	0.5204	8.32	45.988	-0.973
0.0376	0.8723	1302.9	1.1365	6.7529	0.5185	6.64	46.219	-0.726
0.0470	0.8730	1307.2	1.1412	6.7038	0.5166	5.60	46.455	-0.578
0.0564	0.8737	1311.5	1.1458	6.6546	0.5147	4.91	46.688	-0.479

Table 6. Ultrasonic velocity and other acoustic parameter of copper soap derived from treated Mustard oil for 15 Minute. (CM$_{15}$)

c (mol l^{-1})	ρ (g dm^{-3})	u (m s^{-1})	Z $\times 10^{-5}$ (g cm^{-2} s^{-1})	$\beta_{ad} \times 10^{11}$ (cm^2 dyne^{-1})	L_f (A°)	$-\phi_k \times 10^8$	R $\times 10^{-2}$	$S_n \times 10^{-3}$
0.0021	0.8692	1273.9	1.1073	7.0895	0.5313	21.009	45.196	-13.789
0.0041	0.8693	1278.0	1.1110	7.0433	0.5296	19.940	45.280	-6.840
0.0052	0.8694	1280.0	1.1129	7.0202	0.5287	19.715	45.323	-5.450
0.0104	0.8698	1284.1	1.1169	6.9726	0.5269	12.734	45.462	-2.707
0.0156	0.8702	1288.2	1.1210	6.9246	0.5251	10.478	45.598	-1.792
0.0207	0.8707	1292.4	1.1253	6.8762	0.5232	9.396	45.730	-1.334
0.0311	0.8714	1296.6	1.1299	6.8260	0.5213	6.751	45.958	-0.885
0.0415	0.8723	1300.8	1.1347	6.7750	0.5194	5.477	46.179	-0.660
0.0519	0.8732	1305.1	1.1396	6.7240	0.5174	4.717	46.397	-0.525
0.0622	0.8741	1309.3	1.1445	6.6733	0.5155	4.204	46.616	-0.435

Table 7. Ultrasonic velocity and other acoustic parameter of copper soap derived from treated Groundnut oil for 60 Minute (CG_{60})

c (mol l^{-1})	ρ (g dm^{-3})	u (m s^{-1})	Z ×10^{-5} (g cm^{-2} s^{-1})	β_{ad} × 10^{11} (cm^2 dyne^{-1})	L_f (A°)	$-\phi_k$ × 10^8	R × 10^{-2}	S_n × 10^{-3}
0.0022	0.8690	1271.9	1.1053	7.1138	0.5322	8.138	45.182	-13.284
0.0043	0.8693	1273.9	1.1074	7.0889	0.5313	8.435	45.235	-6.616
0.0054	0.8695	1275.9	1.1094	7.0643	0.5304	10.913	45.268	-5.268
0.0108	0.8703	1282.1	1.1157	6.9909	0.5276	10.917	45.409	-2.602
0.0162	0.8712	1286.2	1.1205	6.9391	0.5256	9.646	45.519	-1.720
0.0216	0.8715	1290.3	1.1246	6.8916	0.5238	8.620	45.657	-1.281
0.0325	0.8719	1294.5	1.1287	6.8441	0.5220	6.046	45.900	-0.851
0.0433	0.8722	1298.7	1.1327	6.7978	0.5202	4.707	46.151	-0.636
0.0541	0.8727	1302.9	1.1370	6.7502	0.5184	3.954	46.392	-0.507
0.0649	0.8729	1307.2	1.1410	6.7048	0.5167	3.387	46.647	-0.421

Table 8. Ultrasonic velocity and other acoustic parameter of copper soap derived from treated Mustard oil for 60 minutes (CM_{60})

c (mol l^{-1})	ρ (g dm^{-3})	u (m s^{-1})	Z ×10^{-5} (g cm^{-2} s^{-1})	β_{ad} × 10^{11} (cm^2 dyne^{-1})	L_f (A°)	$-\phi_k$ × 10^8	R × 10^{-2}	S_n × 10^{-3}
0.0020	0.8693	1273.9	1.1073	7.0891	0.5313	21.892	45.193	-14.102
0.0041	0.8697	1278.0	1.1114	7.0408	0.5295	21.602	45.265	-6.989
0.0051	0.8698	1282.1	1.1151	6.9947	0.5277	25.810	45.327	-5.543
0.0101	0.8704	1286.2	1.1195	6.9452	0.5259	16.236	45.455	-2.751
0.0152	0.8710	1290.3	1.1238	6.8960	0.5240	13.020	45.582	-1.820
0.0203	0.8714	1294.5	1.1280	6.8486	0.5222	11.252	45.720	-1.356
0.0304	0.8717	1298.7	1.1321	6.8018	0.5204	7.774	45.972	-0.901
0.0406	0.8720	1302.9	1.1361	6.7555	0.5186	6.015	46.225	-0.673
0.0507	0.8723	1307.2	1.1403	6.7086	0.5168	4.991	46.473	-0.536
0.0609	0.8727	1311.5	1.1445	6.6622	0.5150	4.292	46.723	-0.445

The decrease in intermolecular free length L_f with increase in soap concentration indicates that there is significant interaction between soap and solvent molecules. The decrease in adiabatic compressibility of the soap solutions with increasing soap concentration may be explain on the basis of the that the soap molecules are surrounded by a layer of solvent molecules firmly bounded. This results in the increase in the internal pressure and in lowering the compressibility of the solution *i.e.* solution becomes harder to compress. The above findings may be supported by the fact that as the concentration of solute increases, a larger portion of solvent molecules are electostricted and the amount of bulk solvent decreases causing the compressibility to decrease. In the present study, du/dc is negative which indicates the electrostriction of solvent molecule[24].

The variation in the solvation number with concentration is in fairly good agreement with the results proposed by various workers[25] for the solution of lanthanum nitrate in methanol and ethanol. The values of molar sound velocity R increase linearly with increase in soap concentration. The values of du/dc for copper soaps are positive showing resemblance with the results of other workers[26].

3.2. Micellar Features

The plots of *u, Z, β* and L_f *versus* c show break at a particular soap concentration, which corresponds to the CMC of these soaps (Fig. 1-4). At the CMC hydrocarbon chain structure of soap molecule allows extensive contact between adjacent chains due to change in vibrational and rotational degree of freedom of methylene group. The values of CMC of these soaps are recorded in Table-9. From the Table-9, it is clear that CMC follows the order:

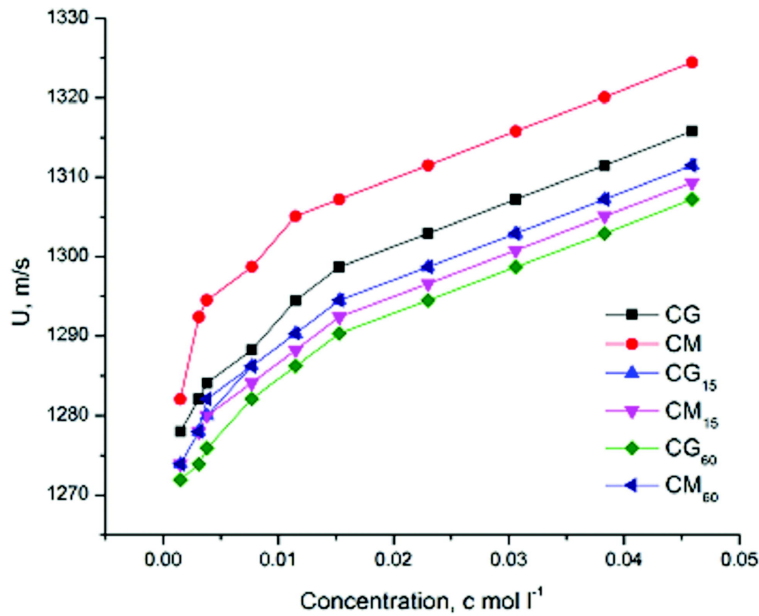$$CG > CM, \quad CG_{15} < CM_{15}, \quad CG_{60} > CM_{60}$$

Fig. 1. Plots of *u* versus *c* for copper soaps derived from treated and untreated groundnut and mustard oils at high temperatures in benzene.

Fig. 2. Plots of *z* versus *c* for copper soaps derived from treated and untreated groundnut and mustard oils at high temperatures in benzene.

Fig. 3. Plots of β_{ad} versus c for copper soaps derived from treated and untreated groundnut and mustard oils at high temperatures in benzene.

Fig. 4. Plots of L_f versus c for copper soaps derived from treated and untreated groundnut and mustard oils at high temperatures in benzene.
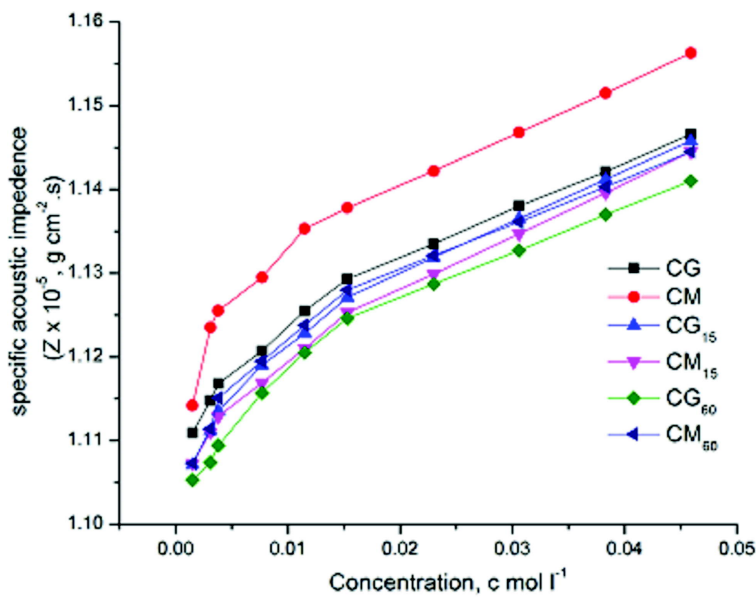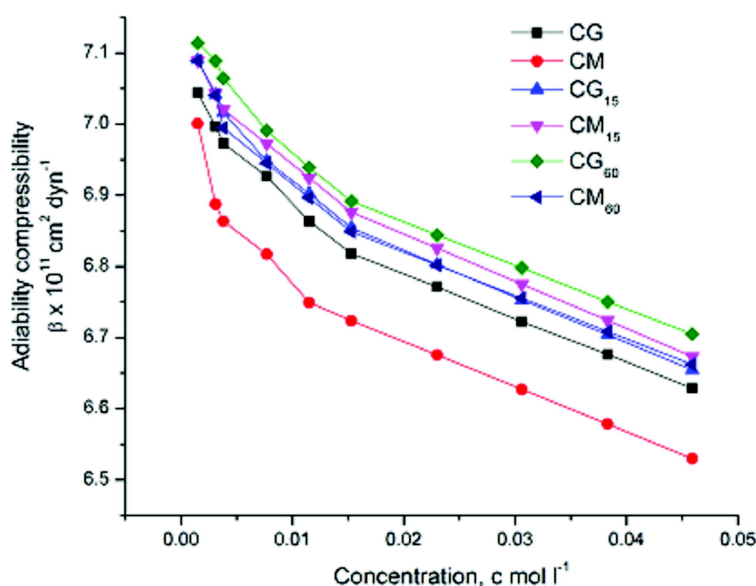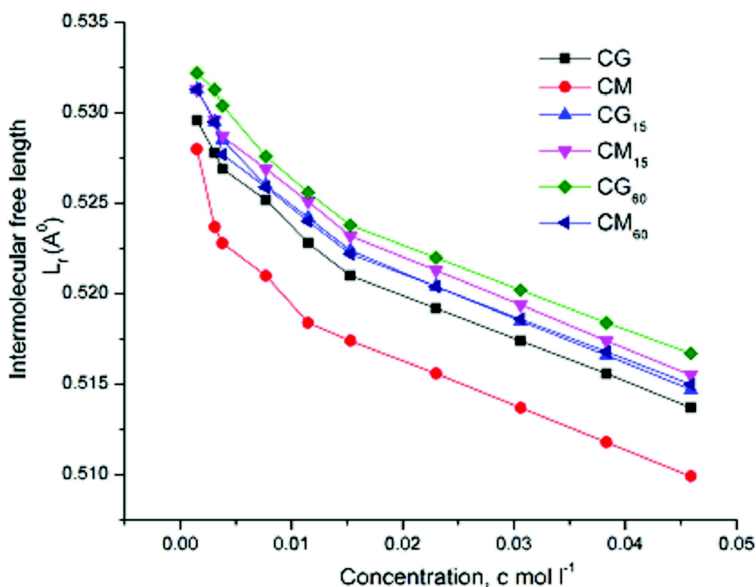
The variation of the ultrasonic velocity with soap concentration c is expressed by the equation:

$$u = u^0 + Gc \tag{12}$$

Here u_0 is the ultrasonic velocity in the solvent. Here G is Gruneisen constant[27]. The value of G is obtained from the slope of the linear plots of u *versus* c below CMC. The plots of ultrasonic velocity versus soap concentration (Fig-1) are extrapolated to zero soap concentration. It is found that the extrapolated values of ultrasonic velocity is in agreement with the experimental value of the velocity in the solvent, indicating that the soap molecules do not aggregate to an appreciable extent below CMC[28].

Table 9. Values of CMC of Copper soaps derived from untreated and treated oils.

Plot	Name of the soap					
	CG	CM	CG_{15}	CM_{15}	CG_{60}	CM_{60}
u versus c	0.0115	0.0105	0.0135	0.0155	0.0165	0.0150
Z versus c	0.0115	0.0105	0.0135	0.0155	0.0165	0.0150
β_{ad} versus c	0.0115	0.0105	0.0135	0.0155	0.0165	0.0150
L_f versus c	0.0115	0.0105	0.0135	0.0155	0.0165	0.0150
ϕ_k versus $\sqrt{c}$	0.012	0.011	0.0139	0.0154	0.0164	0.0151

It is interesting to point out those values of the parameters u, Z, β_{ad} and L_f with respect to copper soaps of different untreated and treated oils follow the order:

[u] CM > CG   [u] : CG_{15} > CM_{15} [u] $\Rightarrow$ CM_{60} CG_{60}

[Z] CM > CG   [Z] : CG15 > CM15   [Z] CM_{60} > CG_{60}

[β] CM < CG   [β] CG_{15} < CM_{15} [β_{ad}] CM_{60} < CG_{60}

[Lf] CM< CG   [L_f] CG_{15} < CM_{15} [Lf] CM_{60} < CG_{60}

The comparison of results for copper soaps of untreated and treated oils suggests that the values of u and Z follow the order:

$$CG > CG_{15} > CG_{60}$$
$$CM > CM_{15} > CM_{60}$$

As observed, the values of ϕ_k increase sharply up to the critical micelle concentration and after CMC it increases gradually. ϕ_k is a function of concentration and its value is found to be in good agreement with that obtained from the following Masson equation [29].

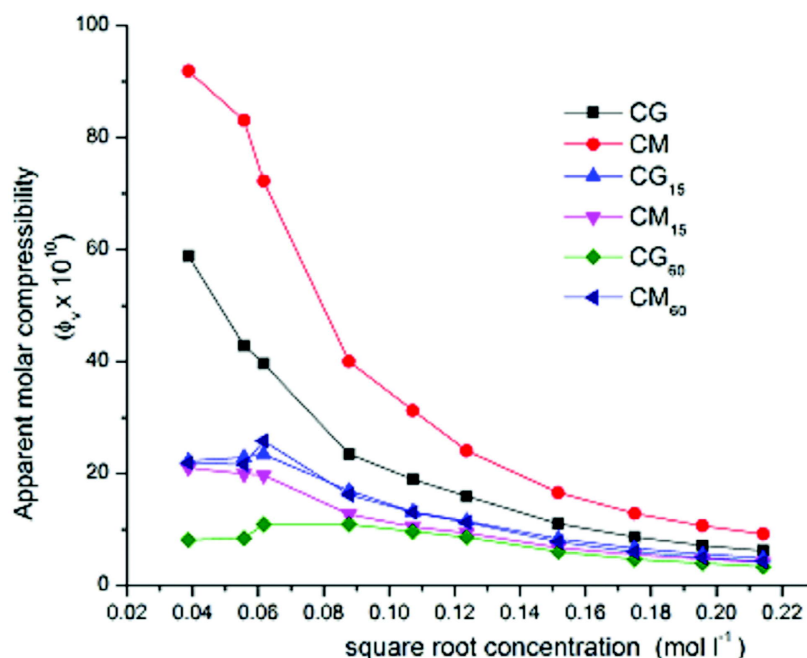$$\phi_k = \phi^0_k + S_k\sqrt{c} \qquad (13)$$

Fig. 5. Plots of ϕ_k versus $\sqrt{c}$ for copper soaps derived from treated and untreated groundnut and mustard oils at high temperatures in benzene.

Where ϕ_k is the limiting apparent molar compressibility and S_k is a constant. The plots of apparent molar compressibility ϕ_k against square root of soap concentration $\sqrt{c}$ are characterized by the intersection of two straight lines at the CMC (Fig. 5). Values of $\phi°_k$ are evaluated from the intercepts of the linear plots of ϕ_k versus $\sqrt{c}$ and values of S_k are calculated from the slope of these plots. In view of the two intersecting straight lines for ϕ_k versus $\sqrt{c}$ plots, it is reasonable to determine two values of parameters $\phi°_k$ and S_k below and above CMC designated as $\phi°_{k1}$, S_{k1} and $\phi°_{k2}$, S_{k2} respectively and recorded in Table 10. From the Table 10, it is clear that the values of $\phi°_{k1}$ and $\phi°_{k2}$ are negative for all these copper soaps. The negative ϕ_k values may be due to the loss of compressibility of solvent due to strong electrostrictive forces in the vicinity of ions [30]. The change in the values of $\phi°_k$ and S_k below and above CMC suggests that there is a phenomenal change in the micellarformation.

Table 10. Values of various constants obtained from Masson's equation for Copper soaps derived from treated and non-treated oils in benzene

Name of the soap	$u_0 \times 10^{-5}$	$G \times 10^{-5}$	$\phi°_{k1} \times 10^8$	$\phi°_{k2} \times 10^8$	$S_{k1} \times 10^8$	$S_{k2} \times 10^8$
CG	1275.5	1.6642	-73.0	-23.0	2.1445	0.3345
CM	1287.0	1.6642	-141.0	-34.0	4.7046	0.4877
CG_{15}	1270.5	1.6318	-33.0	-21.5	0.7002	0.3057
CM_{15}	1272.0	1.1917	-30.0	-17.0	0.6248	0.1943
CG_{60}	1267.0	1.1503	-13.0	-14.5	0.1051	0.2308
CM_{60}	1271.5	1.4281	-30.0	-22.0	0.5543	0.3249

The values of limiting apparent molar compressibility ($\phi°_{k1}$ and $\phi°_{k2}$) are negative and are in the following order :

$$\phi°_{k2} > \phi°_{k1} \text{ and } S_{k1} > S_{k2}$$

It is apparent from that CMC values follow the order:

$$CG > CM, \ CG_{15} < CM_{15}, \ CG_{60} > CM_{60}$$

The results suggested there is decrease in the CMC with the increase in average molecular weight of the soap.This order of CMC is same as observed by other physical properties.

4. CONCLUSION

The ultrasonic velocity and other acoustical parameters of copper surfactants derived from Groundnut and Mustard oil with non polar pure benzene shows the intermolecular interaction in constituent molecules. The decrease in adiabatic compressibility of the soap solutions with increasing soap concentration may be explained on the basis of that the soap molecules are surrounded by a layer of solvent molecules firmly bounded. This results in the increase in the internal pressure and in lowering the compressibility of the solution. This provides useful information about the nature of inter molecular forces occurs in the mixture.

5. ACKNOWLEDGMENT

6. REFERENCES

[1]   R. Sharma and A. K. Sharma, 2017. Natural Edible Oils: Comparative Health Aspects of Sesame, Coconut, Mustard (Rape Seed) and Groundnut (Peanut) A Biomedical Approach. *Biomed J. Sci. & Tech Res.* **1**(5), BJSTR.MS.ID.00044.

[2] G. Savaroglu and M. Ozdemir, 2008. Apparent molar volume and apparent molar isentropic compressibility of glycerol in fructose water at different temperature. *J. Mol. Liquids,* **137**, 51-57.

[3] P. Tank, R. Sharma and A. K. Sharma, 2017. A Pharmaceutical approach & Antifungal activities of Copper Soaps with their N & S donor complexes derived from Mustard and Soyabean oils. *Glob. J. Pharmaceu. Sci.* **3**(4), GJPPS.MS.ID.555619.

[4] V. K. Syal, S. Chauhan and R. Gautam, 1998. Ultrasonic velocity measurements of carbohydrates in binarymixtures of DMSO + H$_2$O at 25°C. *Ultrasonics,* **36**, 619-621.

[5] P. Tank, R. Sharma and A. K. Sharma, 2017. Thermal Behaviour and Kinetics of Copper (II) Soaps and Complexes Derived from Mustard and Soyabean Oil. *J. Anal. Pharm. Res.* **4**(2), 1-5.

[6] S. Sharma, R. Sharma and A. K. Sharma, 2017. Synthesis, Characterization, and thermal degradation of Cu (II) Surfactants for sustainable green chem. *Asian J. Green Chem*. **2**(2), 129-140.

[7] A. K. Sharma, S. Sharma and R. Sharma, 2017. Thermal degradation of Cu (II) metallic Soaps and their Characterizations. A Pharmaceutical Application. *Chronicles of Pharmaceutical Science.* **1**(5), 312-319.

[8] S. Sharma, R. Sharma, L. C. Heda and A. K. Sharma, 2017. Kinetic parameters and Photo Degradation studies of Copper Soap derived from Soybean Oil using ZnO as a Photo catalyst in Solid and Solution Phase. *J. Inst. Chemists* (India). **89**(4), 119-136.

[9] A. K. Sharma, M. Saxena and R. Sharma, 2017. Synthesis, spectroscopic and fungicidal studies of Cu (II) soaps derived from groundnut and sesame oils and their urea complexes. *Bulletin of Pure and Applied Sciences.* **36**(2), 26-37.

[10] A.K. Sharma, M. Saxena and R. Sharma, 2018. Synthesis, Spectroscopic and Biocidal activities of environmentally safe Agrochemicals. *J. Biochem. Tech.* **7**(3), 1139-1147.

[11] S. Punitha and R. Uvarani, 2014. Physico-chemical studies on some saccharides in aqueous cellulose solutions at different temperatures- Acoustical and FTIR analysis. *J. Saudi Chem. Soc*. 18, 657-665.

[12] A. Joram, R. Sharma and A. K. Sharma, 2017. Thermal Degradation of Complexes Derived from Copper (II) Groundnut Soap *(Arachishypogaea)* and Copper (II) Sesame Soap *(Sesamumindicum) Z phy chem.* **232**(4), 459–470

[13] V. M. Kagathara, M. R. Sanariya and P. H. Parsania, 2000. Sound velocity and molecular interaction studies on chloroepoxy resins solutions at 30°C. *Eur. Polym. J.* **36**, 2371-2374.

[14] S. Khan, R. Sharma and A. K. Sharma, 2017. Antifungal Activities of Copper Surfactants derived from Neem *(AzadirectaIndica)* and Karanj *(Pongamia pinnata)* Oils: A Pharmaceutical Application. *Glob. J. Pharmaceu. Sci.* **3**(4), GJPPS.MS.ID.555616.

[15] A. K. Dash and R. Paikaray, 2013. Acoustical study on ternary mixture of dimethyl acetamide (DMAC) in diethyl ether and isobutyl methyl ketone at different frequencies. *Phys. Chem. Liq.* **51**(6), 749-763.

[16] R. Sharma, R. Bhutra and S. Khan, 2010. Micellar Behaviour of Copper Surfactants Derived from Fresh (Untreated) Sesame Oil and Used (Treated at High Temperature) Sesame Oil. *Tenside Surf Det.* **47**, 106-112.

[17] A. K. Sharma, M. Saxena and R. Sharma, 2017. Ultrasonic studies of Cu (II) Soaps derived from Mustard and Soybean oils. J. Pure Appl. Ultrason. **39**(3), 92-99.

[18] P. Tank, R. Sharma and A. K. Sharma, 2017. Studies of Ultrasonic and acoustic parameters of complexes derived from Copper (II) surfactant of mustard oil with N and S atoms containing ligands in non-aqueous media (benzene) at 303.15 K. *J. Acous. Soc. Ind.* **44**(2), 87-99.

[19] R. Bhutra, R. Sharma and A. K. Sharma, 2017. Viscometric and CMC studies of Cu(II) surfactants derived from untreated and treated groundnut and mustard oils in non-aqueous solvent at 298.15 K. *J. Inst. Chemists (India).* **90**, 29-47.

[20] R. Bhutra, R. Sharma and A. K. Sharma, 2017. Comparative Studies of Treated & Untreated Oils as Cu (II) Surfactants "ISBN978-3-659-83122-5" *LAP Lambert Academic Publishing Germany*.

[21] V. Sivakumar, R.V. Verma, P.G. Rao and G. Swaminathan, 2007. Studies on the use of power ultrasound in solid liquid myrobal an extraction process. *J. Clean Prod.* **15**, 1813-1818.

[22] S. Khan, R. Sharma and A. K. Sharma, 2017. Ultrasonic studies of Cu(II) Soap derived from seed oil of Pongamia pinnata (Karanj) in non-aqueous binary and ternary systems at 298.15K. *Malaysian J. Chem.* **19**(2), 99-110.

[23] G. Singh and T. S. Banipal, 2008. Partial molar adiabatic compressibilities and viscosities of some amino acids in aqueous glycerol solutions at 298.15K. *Indian J. Chem.* **47A**, 1355-1364.

[24] P. Tank, R. Sharma and A. K. Sharma, 2018. Viscometric Studies of Cu (II) surfactants derived from mustard oil in benzene at 303.15K. *Tenside Surf Det.* In press.

[25] S. V. Ranganayakulu, C. S. Reddy and D.L. Reddy, 2008. Ultrasonic studies of the binary mixtures of ethyl acetate and cresols-application of Kosower and Dimroth Treatments. *Mat. Chem. Phys.* **90**, 213-216.

[26] P. Tank, R. Sharma and A. K. Sharma, 2018. Micellar Features and Various Interactions of Copper Soap Complexes Derived from Edible Mustard Oil in Benzene at 303.15 K. *Curr. Phy. Chem.* **8**(1), 46-57

[27] S. R. Kanhekar, P. Pravina and K. B. Govind, 2010. Thermodynamic properties of electrolytes in aqueous solutions of glycine at different temperatures. *Indian J. Pure Appl. Phys.* **48**, 95-99.

[28] A. K. Sharma, M. Saxena and R. Sharma, 2017. Ultrasonic studies of Cu (II) Soaps derived from Groundnut and Sesame oils. *Tenside. Surf. Det.* **55**(2), 127-134.

[29] D. O. Masson, 1929. Solute molecular volumes in relation to solvation and ionization, *Philos. Mag.*, **8**, 218-235.

[30] A. K. Sharma, M. Saxena, R. Sharma, Ultrasonic studies of Copper Soaps Urea complexes derived from Mustard and Soyabean oils. *J. Phy. Sci.* In press.

INFORMATION FOR AUTHORS

ARTICLES
The Journal of Acoustical Society of India (JASI) is a refereed publication published quarterly by the Acoustical Society of India (ASI). JASI includes refereed articles, technical notes, letters-to-the-editor, book review and announcements of general interest to readers.

Articles may be theoretical or experimental in nature. But those which combine theoretical and experimental approaches to solve acoustics problems are particularly welcome. Technical notes, letters-to-the-editor and announcements may also be submitted. Articles must not have been published previously in other engineering or scientific journals. Articles in the following are particularly encouraged: applied acoustics, acoustical materials, active noise & vibration control, bioacoustics, communication acoustics including speech, computational acoustics, electro-acoustics and audio engineering, environmental acoustics, musical acoustics, non-linear acoustics, noise, physical acoustics, physiological and psychological acoustics, quieter technologies, room and building acoustics, structural acoustics and vibration, ultrasonics, underwater acoustics.

Authors whose articles are accepted for publication must transfer copyright of their articles to the ASI. This transfer involves publication only and does not in any way alter the author's traditional right regarding his/her articles.

PREPARATION OF MANUSCRIPTS
All manuscripts are refereed by at least two referees and are reviewed by the Publication Committee (all editors) before acceptance. Manuscripts of articles and technical notes should be submitted for review electronically to the Chief Editor by e-mail or by express mail on a disc. JASI maintains a high standard in the reviewing process and only accept papers of high quality. On acceptance, revised articles of all authors should be submitted to the Chief Editor by e-mail or by express mail.

Text of the manuscript should be double-spaced on A4 size paper, subdivided by main headings-typed in upper and lower case flush centre, with one line of space above and below and sub-headings within a section-typed in upper and lower case understood, flush left, followed by a period. Sub-sub headings should be italic. Articles should be written so that readers in different fields of acoustics can understand them easily. Manuscripts are only published if not normally exceeding twenty double-spaced text pages. If figures and illustrations are included then normally they should be restricted to no more than twelve-fifteen.

The first page of manuscripts should include on separate lines, the title of article, the names, of authors, affiliations and mailing addresses of authors in upper and lowers case. Do not include the author's title, position or degrees. Give an adequate post office address including pin or other postal code and the name of the city. An abstract of not more than 200 words should be included with each article. References should be numbered consecutively throughout the article with the number appearing as a superscript at the end of the sentence unless such placement causes ambiguity. The references should be grouped together, double spaced at the end of the article on a separate page. Footnotes are discouraged. Abbreviations and special terms must be defined if used.

EQUATIONS
Mathematical expressions should be typewritten as completely as possible. Equation should be numbered consecutively throughout the body of the article at the right hand margin in parentheses. Use letters and numbers for any equations in an appendix: Appendix A: (A1, (A2), etc. Equation numbers in the running text should be enclosed in parentheses, i.e., Eq. (1), Eqs. (1a) and (2a). Figures should be referred to as Fig. 1, Fig. 2, etc. Reference to table is in full: Table 1, Table 2, etc. Metric units should be used: the preferred from of metric unit is the System International (SI).

REFERENCES
The order and style of information differs slightly between periodical and book references and between published and unpublished references, depending on the available publication entries. A few examples are shown below.

Periodicals:
[1] S.R. Pride and M.W. Haartsen, 1996. Electroseismic wave properties, *J. Acoust. Soc. Am.*, **100** (3), 1301-1315.
[2] S.-H. Kim and I. Lee, 1996. Aeroelastic analysis of a flexible airfoil with free play non-linearity, *J. Sound Vib.*, **193** (4), 823-846.

Books:
[1] E.S. Skudzryk, 1968. *Simple and Comlex Vibratory Systems*, the Pennsylvania State University Press, London.
[2] E.H. Dowell, 1975. *Aeroelasticity of plates and shells*, Nordhoff, Leyden.

Others:
[1] J.N. Yang and A. Akbarpour, 1987. Technical Report NCEER-87-0007, Instantaneous Optimal Control Law For Tall Buildings Under Seismic Excitations.

SUMISSIONS
All materials from authors should be submitted in electronic form to the JASI Chief Editor: B. Chakraborty, CSIR - National Institute of Oceanography, Dona Paula, Goa-403 004, Tel: +91.832.2450.318, Fax: +91.832.2450.602,(e-mail: bishwajit@nio.org) For the item to be published in a given issue of a journal, the manuscript must reach the Chief Editor at least twelve week before the publication date.

SUMISSION OF ACCEPTED MANUSCRIPT
On acceptance, revised articles should be submitted in electronic form to the JASI Chief Editor (bishwajit@nio.org)